UNIVERSIDADE FEDERAL DA BAHIA
INSTITUTO DE GEOCIÊNCIAS
PROGRAMA DE PESQUISA E PÓS-GRADUAÇÃO EM GEOLOGIA
ÁREA DE CONCENTRAÇÃO: PETROLOGIA, METALOGÊNESE E
EXPLORAÇÃO MINERAL

DISSERTAÇÃO DE MESTRADO

OCORRÊNCIAS DE GRAFITA NO COMPLEXO TANQUE NOVO - IPIRÁ, NORDESTE DO CRÁTON DO SÃO FRANCISCO, BAHIA, BRASIL: CARACTERIZAÇÃO E POTENCIAL METALOGENÉTICO

IB SILVA CÂMARA

SALVADOR
2021

OCORRÊNCIAS DE GRAFITA NO COMPLEXO TANQUE NOVO - IPIRÁ, NORDESTE DO CRÁTON DO SÃO FRANCISCO, BAHIA, BRASIL: CARACTERIZAÇÃO E POTENCIAL METALOGENÉTICO

Ib Silva Câmara

Orientador: Prof. Dr. Aroldo Misi

Dissertação de Mestrado apresentada ao Programa de Pós-Graduação em Geologia do Instituto de Geociências da Universidade Federal da Bahia como requisito parcial à obtenção do Título de Mestre em Geologia, Área de Concentração: Petrologia, Metalogênese e Exploração Mineral.
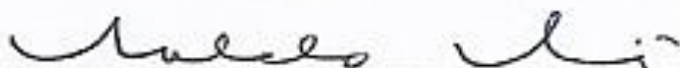
SALVADOR

2021

IB SILVA CÂMARA

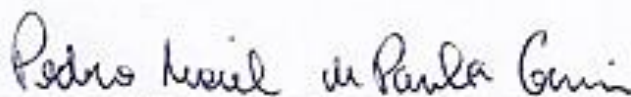# OCORRÊNCIAS DE GRAFITA NO COMPLEXO TANQUE NOVO - IPIRÁ, NORDESTE DO CRÁTON DO SÃO FRANCISCO, BAHIA, BRASIL: CARACTERIZAÇÃO E POTENCIAL METALOGENÉTICO

Dissertação apresentada ao Programa de Pós-Graduação em Geologia da Universidade Federal da Bahia, como requisito para a obtenção do Grau de Mestre em Geologia na área de concentração em Petrologia, Metalogênese e Exploração Mineral em 20/08/2021.

DISSERTAÇÃO APROVADA PELA BANCA EXAMINADORA:

_____
Dr. Aroldo Misi (Orientador) - UFBA

_____
Dr. Pedro Maciel de Paula Garcia - UFMT

_____
Dr. Debora Correia Rios - UFBA

Salvador – BA
2021

Dedico este trabalho a minha família, meus amigos e minha comunidade, pois sempre me apoiaram e me deram a força necessária para continuar lutando e seguindo em frente. A Coordenação de Aperfeiçoamento de Pessoal de Nível Superior – Brasil (CAPES) pelo suporte com bolsa de pesquisa. Ao Grupo de Metalogenese da UFBA, por proporcionar o desenvolvimento deste trabalho com orientações, apoio e incentivo. A Companhia Baiana de Pesquisa Mineral – CBPM pelo financiamento da pesquisa. A toda comunidade científica brasileira que resiste ao caos. A meu professor e orientador Aroldo Misi que é um exemplo de eterno entusiasta e pesquisador da geologia e da vida.

AGRADECIMENTOS

Agradeço por ter os caminhos abertos e continuar seguindo em frente, peço a benção dos meus avós: Valter, Carolina, Creusa e Idaiano. A minha família, por toda a vida, minha mãe Evanilde que sempre lutou bravamente por mim e por minha educação, a meu pai Charles que trabalhou duro em sua jornada, minhas irmãs: Bia (por tantos momentos catastróficos e bonitos), Maria Clara (por conversas na frente da casa de vó Minerva) e Berta (um dia eu entendo o sarcasmo!) e a uma nova mãe Márcia; a Louise, minha esposa e companheira, que está ao meu lado nessa árdua caminhada me ajudando a me levantar toda vez que caio, aguentando toda a ausência devido aos campos intermináveis... te amo muito! Ao meu padrinho Julião e madrinha Eva. Aos meus irmãos de vida, Tone que até minha casa construiu, Mazo (tatuadeiro) e Erick (matemático). A minha comunidade, a casa de Odé que me acolheu, a meu Baba Elson que ajustou meu ori e me fortaleceu para ser o Ibi de Oxalá, a mãe Alda e mãe Meire que me abraçaram!!! Aos irmãos e irmãs que tive a oportunidade de conhecer através da geologia e respirar a vida: Sara (grande irmã para todas as horas!), Carlos (não conheço ninguém mais criativo), Karina (irmã das águas), Pedro (ao ser político e reflexivo!), Rebeca (menina organizada e paciente para aguentar Pedro!), Luis Rodrigues (grande cientista que teve participação fundamental nessa pesquisa) e Tatiana (grande cientista e apoiadora). Ao grupo de metalogênese da UFBA representados pelo professor Haroldo Sá que deu a ideia da pesquisa; a Flori que é uma pessoa incrível com humor e entusiasmos fantásticos!; ao meu professor e orientador Aroldo Misi por toda paciência e apoio para o desenvolvimento da pesquisa, entusiasmos e paciência para enfrentar toda burocracia deste país; a professora Debora pelo apoio. A toda comunidade cientifica da UFBA e da geologia na Bahia, pelo ensino, produção cientifica e enfrentamento de todo o caos e desgoverno. Em especial a professora Simone por aguentar a burocracia e os trabalhos intermináveis que a pós-graduação exigem. A Companhia Baiana de Pesquisa Mineral – CBPM pelo financiamento da pesquisa. Tenho amor por todos que citei nesse curto agradecimento! Bàbá esà rè wa!! Xeuê Baba!!!

RESUMO

O Brasil é o terceiro maior produtor de grafita do mundo, ocupando o estado da Bahia, o ranking de segundo maior produtor do país sendo a maior parte da produção oriunda da Província Grafítica Bahia-Minas, no contexto geológico do Orógeno Araçuai. Além desta, diversas regiões da Bahia registram ocorrências de grafita, como a área de estudo que localiza-se 350 km a norte dessa província e se situa no contexto tectônico do Complexo Tanque Novo–Ipirá (CTNI), Orógeno Itabuna-Salvador-Curaçá, nordeste do Cráton do São Francisco. A área de estudo é constituída por rochas metassedimentares, onde as rochas hospedeiras são xistos, mármores e granulito tendo como encaixantes quartzitos, calcissilicáticas, mármores e formações ferríferas do CTNI. As análises petrográficas, com auxílio do MEV/EDS, apontam duas gerações de grafita: a primeira é associada ao processo de grafitização gerada pelo metamorfismo, sendo classificada como singenética apresentando flakes com três associações distintas relacionados ao metamorfismo progressivo de fácies xisto verde, anfibolito e granulito; Já a segunda geração, epigenética, é atribuída ao retrometamorfismo com percolação de fluidos hidrotermais atribuídos ao fácies xisto-verde com deposição de grafita em vênulas ou como resultado de reações de carbonatação. Os corpos grafitosos apresentam um alto Teor de Carbono Grafítico (TCG), analisados por infravermelho em LECO, variando de 8,70% a 15,98% e ocorrem em dois grupos distintos: aluminoso (paragnaisse e xisto) e carbonático (mármore). A litogeoquímica indica protólitos sedimentares com assinaturas influenciadas por aporte detrítico em um paleoambiente marinho, com alterações diagenéticas, mas que não foram suficientes para alterar as anomalias de Ce/Ce* (0,64 a 1,49) e U/Th (0,04 a 1,30) que sugerem um paleoambiente predominantemente óxico. Nas hospedeiras o Cg é correlacionável com as razões P/Ti, Ba/Ti, Ni e Cu o que sugere a deposição da matéria orgânica em um momento de alta paleoprodutividade orgânica. Essa configuração deposicional pode indicar que a deposição da matéria orgânica que originou a grafita resulte do aumento da paleoprodutividade gerada após o evento GOE (Grande Evento de Oxigenação), que culminou no primeiro grande evento fosfogenético do registro geológico. Essa dissertação representa uma primeira caracterização para as mineralizações de grafita do CTNI.

Palavras-chave: Mineralização de Grafita, Carbono grafítico, Paleoprodutividade, Paleoproterozoico

ABSTRACT

Brazil is the third biggest producer of graphite worldwide, with the state of Bahia being the second largest producer in the country, as most of the production comes from the Graphite Province of Bahia-Minas. The study area is situated at 350 km to the north of this producing region, in the Tanque Novo-Ipirá Complex, Itabuna-Salvador-Curaçá Orogen, São Francisco Craton. The area is comprised of host rocks with occurrences of graphite such as schists, marbles, and granulites as well as country rocks characterized by quartzites, calc-silicate rocks, marbles, and iron formations. The petrographic analysis supported by MEV/EDS indicates two generations of graphite: the first one, connected to the graphitization process generated by metamorphism (syngenetic), exhibit flakes with three distinct associations related to the greenschist, amphibolite, and granulite facies in which the host rocks were subjected; and the second generation, is related to the percolation of hydrothermal fluids (epigenetic) due to retrograde metamorphism in the greenschist facies that promoted the deposition of graphite in venules or as a result of carbonation. The graphite bodies show a high total graphitic carbon (TGC), analyzed by LECO infrared, ranging from 8.70 to 15.98wt% and they occur in two distinct lithologies: aluminous and carbonate. The geochemical characteristics of the host and country rocks indicate sedimentary protoliths with signatures influenced by diagenetic alterations and detrital input in a marine paleoenvironment. However, they were not sufficient to change the anomalies of Ce/Ce* (0.64 to 1.49) that alongside the ratios of U/Th (0.04 to 1.30) suggest a paleoenvironment dominantly oxic. The analyzes of TGC with P/Ti, Ba/Ti, Ni and Cu show correlations that suggest the deposition of organic matter in a context of high organic paleo productivity. This depositional setting combining with the phosphorus anomalies in the country rocks, deposited during the Paleoproterozoic in an oxic paleoenvironment, suggest that the deposition of organic matter that originates the graphite might be related to the increase in paleo productivity generated following the Great Oxygenation Event (GOE), which culminated in the first major phosphogenesis event in the geological record

Keywords: Graphite, total graphitic carbon, paleo productivity, Paleoproterozoic.

SUMÁRIO

CAPÍTULO 1 - INTRODUÇÃO GERAL

O termo grafita deriva da palavra grega graphein (escrever) e descreve um mineral caracterizado por baixa dureza e peso específico, é altamente refratário, com ponto de fusão acima de 3600 °C, é inerte quimicamente tendo resistência a corrosão, um excelente lubrificante e apresenta a maior condutividade térmica e elétrica dos não-metais (Pierson, 1993; Klein & Dutrow, 2012).

Os átomos de carbono na grafita estão organizados em anéis de 6 membros nos quais cada átomo de carbono tem três vizinhos próximos ordenados no sistema hexagonal. O conjunto desses anéis ordenados forma lâminas conhecidas como grafeno, que, por sua vez, estão empilhadas no sentido paralelo ao eixo cristalográfico "c". Existem dois tipos de arranjos espaciais para o empilhamento das camadas de grafeno possíveis: a sequência ABABAB... que caracteriza a estrutura hexagonal da grafita, mais frequente, e a sequência ABCABC... que forma a estrutura romboédrica (Klein & Dutrow, 2012; Kwiecinskaa & Petersen, 2004; Figura 1). A estrutura da grafita aqui descrita representa um modelo ideal, contudo, na natureza encontrar tal estrutura bem cristalizado é possível apenas em poucos ambientes geológicos. Outros nomes para designar materiais intermediários entre a matéria carbonosa e o mineral grafita completamente ordenado, são semi-grafita (Kwiecinskaa & Petersen, 2004) e carbono grafítico (Busseck & Beyssac, 2014).

A formação do mineral grafita está intimamente relacionada ao ciclo do carbono, sendo a maior parte desse mineral gerada pela concentração de biomassa em sedimentos e posterior metamorfismo destes, processo denominado de grafitização (Beyssac & Rumble, 2014). A grafitização consiste na polimerização e rearranjo estrutural de conjuntos aromáticos para a sequência termodinamicamente estável da grafita, o empilhamento ABAB... (Beyssac & Rumble, 2014). Outras reações para a formação da grafita também são descritas na literatura como: emanações gasosas, descarbonatação, liberação de CO_2 em processos de silicificação, dissociação do metano e precipitação a partir de fluidos contento C-O-H (Clark, 1921; French & Rosenberg, 1965; Salotti et al. 1971; Ridge, 1976; Kwiecinska & Petersen, 2004).
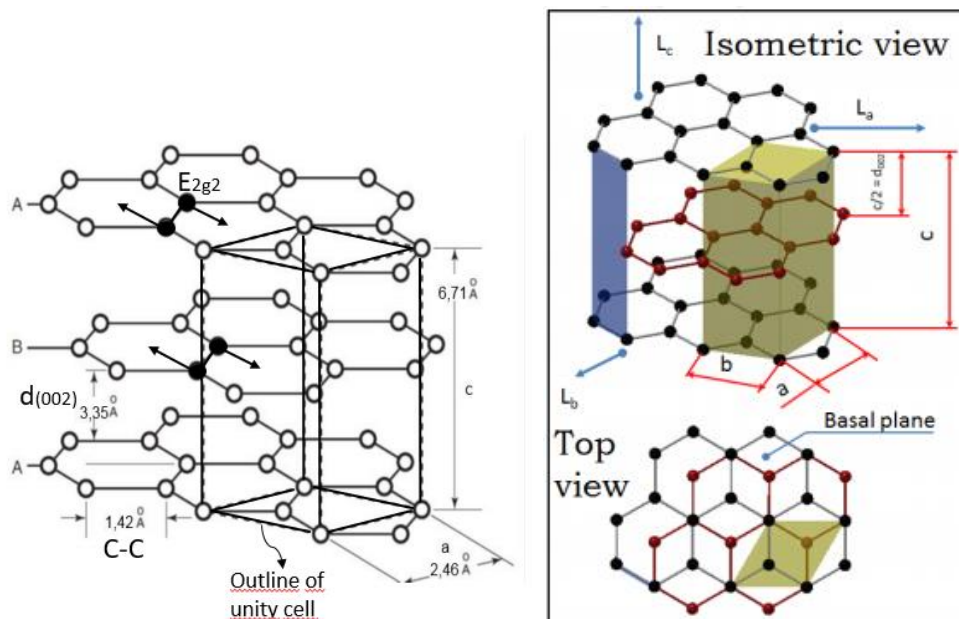
Figura 1: Ilustração do cristal hexagonal de grafita e os parâmetros da célula unitária (a e c). La: Diâmetro médio de empilhamento; Lc: Altura do Empilhamento; $d_{(002)}$: Distância interplanar. (Fonte: Kwiecinskaa & Petersen, 2004)

As ocorrências de grafita analisadas nesse trabalho localizam-se no nordeste do Brasil, estado da Bahia, e do ponto de vista geológico no Complexo Tanque-Novo-Ipirá (CTNI), unidade metavulcano sedimentar representante de uma bacia polifásica de idade paleoproterozóica-neoarqueana integrante do Orogeno Salvador-Curaçá, Cráton do São Francisco (CSF; Kosin et al. 1993; Ribeiro, 2017). Esse complexo exibe a presença de um conjunto litológico e ocorrências de grafita, fosfato, mármores e quartzitos semelhantes ao encontrado em séries khondalíticas como Kalahandi, India (Walker, 1902); Orissa, Índia (Dash et al. 1987; Bhattacharya, 2012); Craton do Norte da China (Wang et al. 2011; Liu et al. 2016; Zhong et al. 2019); e Rio de Janeiro, Brasil (Pereira & Guimarães, 2012). A presença de importantes deposito de grafita nesses complexos khondalíticos (Ji et al. 1994), principalmente na China e Índia, apontam para um elevado potencial metalogenetico do CTNI.

Na Figura 2, pode-se observar as principais ocorrências de grafita mapeadas pelo Serviço Geológico do Brasil (CPRM) e notar que a área de estudo situa-se a norte da Província Grafítica Bahia-Minas (Pedrosa-Soares et al. 1999; Belem, 2006; Daconti, 2004). Essa província localiza-se no contexto do Orógeno Araçuaí, faixa Neoproterozóica que limita a borda sudeste do CSF, registrando 3 minas distrivuídas nas cidades: de Maiquinique, Pedra Azul e Salto da Divisa além de 1 deposito bem delimitado nas cidades

de Itabela/Eunápolis. A quarta mina brasileira ocorre no sul do CSF, na cidade de Itapecerica, em rochas arqueanas-paleoproterozóicas (Teixeira et al. 2017).

Esse estudo representa uma primeira caracterização das mineralizações de grafita no CTNI tendo como foco a descrição das rochas hospedeiras e encaixantes da mineralização, grau de oxigenação e condições paleoambientais, descrição dos processos metalogenéticos formadores dos depósitos de grafita, sua relação com ocorrências de fosfato e consequentes implicações em relação ao Grande Evento de Oxigenação (GOE).
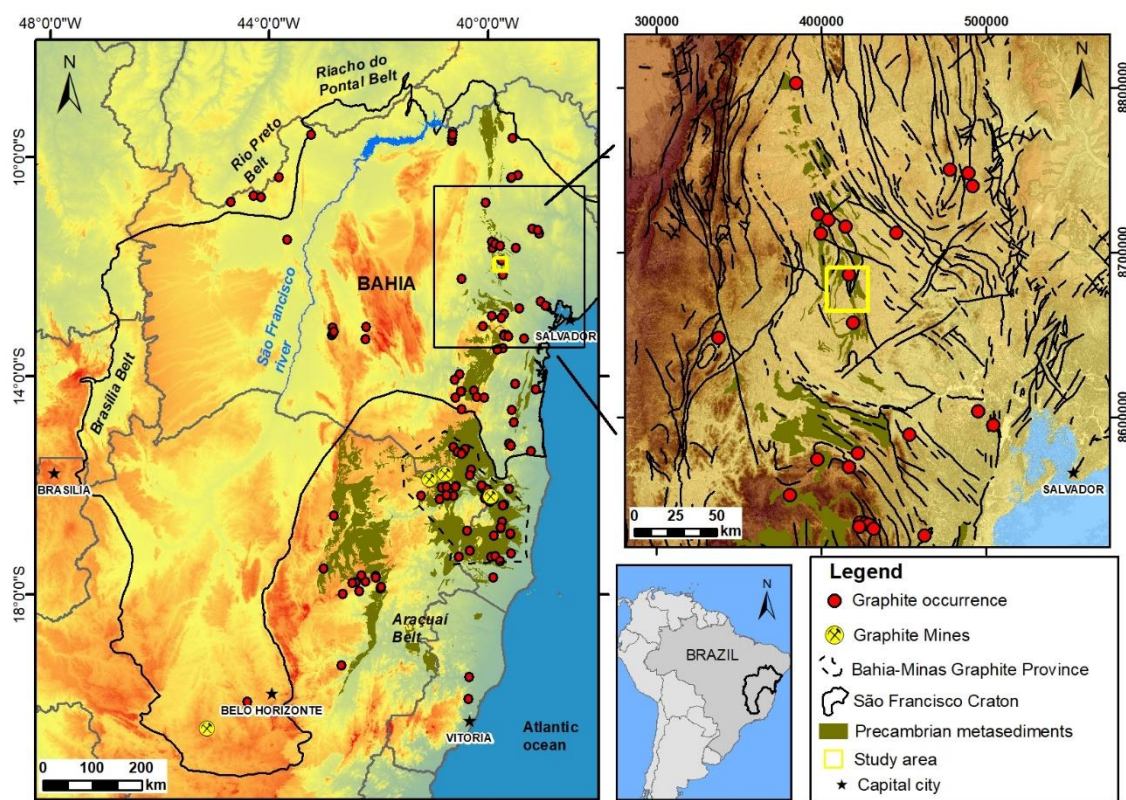
Figura 2: Mapa de localização da área de estudo em relação a Província grafítica Bahia-Minas.

A grafita é, atualmente, considerada no mundo um mineral estratégico. Isso se deve, principalmente, às suas características físico-químicas que a torna versátil possuindo diversos usos. Tem-se observado um constante aumento no preço dessa commodity, devido a fatores como: as regulações ambientais na China levando ao fechamento de algumas minas; e ao aumento na demanda da indústria de tecnologia a exemplo da aplicação de grafita como anodo nas baterias de lítio utilizadas em veículos elétricos, sendo esperado um aumento de 10 vezes esta demanda até o ano de 2025 (Scherba et al. 2018: Jara et al. 2019). Notícias sobre as inovações tecnológicas advindas da descoberta do grafeno e do aumento da demanda de oxido de grafeno (GO) tem gerado

especulações no mercado e produz, um consequente aumento no preço da grafita (Heider, 2017; Boggild, 2018; Siow, 2017).

O minério de grafita é classificado em três tipos de depósitos: veio (também conhecido como lump ou chip), amorfo (grafita microcristalina) e flake. Estima-se, atualmente, que a produção global média de grafita natural seja da ordem de 1.2Mt por ano. Destes 600 – 800k sejam de grafita flake, 300kt de grafita amorfa e 4kt de grafita em veio (Scogings, 2019). Os principais usos são refratários (28%), baterias (18%), cadinhos (17%), lubrificantes (10%), aditivo de carbono (5%) e outros (22%; Scherba et al. 2018). Os maiores produtores mundiais de grafita são: China (66%), seguida por Índia (14%) e pelo Brasil (7%; Keeling, 2017). Apesar da produção de grafita natural a grafita sintética representa cerca de 90% do mercado que foi estimado em 14 bilhões de dólares no pico da demanda em 2012, tendo uma produção de cerca de 1.5Mt por ano, sendo os principais produtores China e Estados Unidos (Jara et al. 2019; Keeling, 2017).

Comercialmente a grafita natural é classificada de acordo com dois principais fatores: (1) tamanho do flake variando de muito fino ou amorfo (<0,075 mm ou -200 mesh), fino (0,075 – 0,15 mm ou 100 – 200 mesh), médio (0,15 – 0,3 mm ou 80 – 100 mesh), coarse large (0,18 – 0,3 ou 48 – 80 mesh), coarse jumbo (>0,3 mm ou +48 mesh); e (2) total graphite content – TGC (%) que varia de classes de 88 – 93%, 94 -95% e 95 – 97%. Especificidades técnicas para uso também influenciam no preço do minério, a exemplo: conteúdo volátil, umidade, densidade total, cristalinidade, área superficial especifica, impurezas, temperatura pico de oxidação e volume de expansão (Scogings, 2019; Jara et al. 2019; Keeling, 2017).

Essa dissertação foi gerada no formato artigo, apresentando uma breve introdução sobre o tema de pesquisa, o artigo submetido na Brazilian Journal of Geology. A revista proposta atende aos requisitos estabelecidos pelo Programa de Pós-Graduação em Geologia - PPGEO. No ANEXO A, encontram-se as regras de formatação de submissão da revista. O apêndice A estão justificados os motivos pela presença dos coautores.

Referências

Bhattacharya S, Choudhary AK, Basei, M. 2012. Original nature and source of khondalites in the Eastern Ghats province, India. In: Mazumder R, Saha D (eds) Palaeoproterozoic of India. Geol Soc Lond Spec Publ 365:145–158.

Belém, J. 2006. Caracterização mineralógica, física e termobarométrica de minérios de grafita da Província Grafítica Bahia-Minas. Dissertação de Mestrado, Instituto de Geociências, Universidade Federal de Minas Gerais, 165 p.

Beyssac, O. & Rumble, D. 2014. Graphitic carbon: A Ubiquitous, Diverse, and Useful Geomaterial. Elements. 10:415–420.

Boggild, P. 2018. The war on fake graphene. Nature 562, 502-503. DOI: 10.1038/d41586-018-06939-4.

Buseck P.R., Beyssac, O. 2014. Graphitic carbon: from organic matter to graphite: graphitization. Elements. 10:421–426.

Clark, 1921. The Origin of Graphite. Economic Geology, 16 (3), pp. 167 – 183.

Daconti B.C. 2004. Contexto geologico, controle e correlação regional das mineralizações de grafita da região de almenara, Província grafítica do nordeste de Minas Gerias. Dissertação de Mestrado, Instituto de Geociências, Universidade Federal de Minas Gerais, 95p.

Dash, B., Sahoo, K. N. and Bowes, D. R. 1987. Geochemistry and original nature of Precambrian khondalites in the Eastern Ghats, Orissa, India. Transactions of the Royal Society of Edinburgh, Earth Science, 78, 115–127.

French, B.M., Rosenberg, P.E., 1965. Siderite (FeCO3): thermal decomposition in equilibrium with graphite. Science 147, 1283– 1284.

Heider, M. Potencialidades da cadeia produtiva de grafeno no Brasil: do recurso mineral ao grafeno. In the mine, Facto editorial, 2017. n° 65, 34 p.

Jara, A. D., Betemariam, A., Woldetinsae, G., Kim, J. Y. 2019. Purification, application and current market trend of natural graphite: A review. International Journal of Mining Science and Technology. Vol. 29, p. 671–689.

Ji, H., Shimazaki, H., Hu, S., Zhao, Y. 1994. Occurrence and geochemistry of khondalite series in the Shandong Peninsula, China. Resource Geology, 44(1), p. 39-49.

Klein, C. and Dutrow, B. 2012. Manual de Ciência dos Minerais, 23a ed. Bookman.

Keeling, J., 2017, Graphite: Properties, uses and south Australian resources: MESA Journal, v. 84, p. 28–41.

Kosin, M. D., Melo, R.C., Souza, J.D., Oliveira, E.P., Carvalho, M.J.; Leite, C.M.M. 2003. Geologia do segmento norte do Orógeno Itabuna-Salvador-Curaçá e guia de excursão. Revista Brasileira de Geociências, São Paulo, 33(1): 15-26.

Kwiecińska, B., and Petersen, H.I., 2004. Graphite, semi-graphite, natural coke, and natural char classification—ICCP system. International Journal of Coal Geology, 57, 99-116.

Liu, F.L., Liu, P.H., Cai, J. 2016. Genetic Mechanism and Metamorphic Evolution of Khondalite Series Within the Paleoproterozoic Mobile Belts, North China Craton. M.

Zhai et al., (eds.), Main Tectonic Events and Metallogeny of the North China Craton, Springer Geology, DOI 10.1007/978-981-10-1064-4_8.

Pedrosa-Soares A.C., Faria L.F., Reis L.B. 1999. The Minas-Bahia Graphite Province, eastern Brazil: mineralization controls and types. In: European Union Geosciences, Strasbourg. Abstract H04: 4A/09: F5, p. 493.

Pereira, R.M. and Guimarães, P.A., 2012. A Faixa Khondalítica Marangatu e a descoberta de novas mineralizações de grafita no N-NW do Estado do Rio de Janeiro. Geociências, 31(2): 197-205.

Pierson, H. O. 1993. The Element Carbon. Handbook of Carbon, Graphite, Diamonds and Fullerenes, 11–42. doi:10.1016/b978-0-8155-1339-1.50007-4.

Ribeiro, T. S. 2017. Complexo Tanque Novo-Ipirá: geologia e potencialidade para fosfato na folha pintadas, Bahia. Org. Miranda, L. L. F. CBPM. Série arquivos abertos, n 42, 94 p. ISBN 978-85-85680-57-2.

Ridge, J.D, 1976. Annotated Bibliographies of Mineral Deposits in Africa, Asia (exclusive of the USSR) and Australia. The Pennsylvania State University, College of Earth and Mineral Sciences, Pennsylvania.

Salotti, C.A.; Heinrich, E.W.; Giardini, A. A. 1971. Abiotic Carbon and the Formation of Graphite Deposits. Economic Geology Economic Geology. Vol. 66, 1971, pp. 929-932.

Scherba, C., Montreuil, J.F., Barrie, C. T. 2018. Geology and Economics of the Giant Molo Graphite Deposit, Southern Madagascar. Society of Economic Geologists, Inc. SEG Special Publications, no. 21, pp. 347–363.

Scogings, A. 2019. Graphite Mineral Notes - geology, petrography, production, markets, specifications. Published on LinkedIn.

Siow, K. S. Graphite Exfoliation to Commercialize Graphene Technology, Sains Malaysiana, 46 (7), 2017, 46(7), pg 1047-1059. DOI: 10.17576/jsm-2017-4607-06.

Teixeira, W., Oliveira E. P., Peng, P., Dantas, E. L., Hollanda, M. H. B. M. 2017. U-Pb geochronology of the 2.0 Ga Itapecerica graphite-rich supracrustal succession in the São Francisco Craton: Tectonic matches with the North China Craton and paleogeographic inferences. Precambrian Research vol. 293 p. 91–111.

Walker, T. L. 1902. The geology of Kalahandi State, Central Provinces, India. U.S. Geol. Surv. Memoirs, 33, part 3.

Wang, F., Li, X.P., Chu, H., Zhao, G. 2011. Petrology and metamorphism of khondalites from the Jining complex, North China craton, International Geology Review, 53:2, 212-229, DOI: 10.1080/ 00206810903028144.

Zhong, Y., Ma, X.D., Li, H.K., Zhaid M.G. 2019. Revisit and comparative analysis of the typical graphite deposits in the Paleoproterozoic khondalite series, western North China Craton: Implications for genesis, depositional environment and prospecting potential. Ore Geology Reviews, v. 109, p. 370–380.

CAPÍTULO 2 - ARTIGO 1: GRAPHITE OCCURRENCES IN THE TANQUE NOVO - IPIRÁ COMPLEX, NORTHEAST OF THE SÃO FRANCISCO CRATON, BAHIA, BRAZIL: CHARACTERIZATION AND METALLOGENIC POTENTIAL

Geological and geochemical characterization and metallogenetic implications of graphite occurrences in the Tanque Novo - Ipirá Complex, Northeast São Francisco Craton, Bahia, Brazil

Ib Silva Câmara[1], Aroldo Misi[2], Luís Rodrigues dos Santos de Oliveira[1], Tatiana Silva Ribeiro[1], José Haroldo da Silva Sá[2], Herbet Conceição[3], Pedro Ribeiro Rabelo de Santana[1] Pedro Maciel de Paula Garcia[4]

(1) Programa de Pós-Graduação em Geologia. Instituto de Geocisências, Universidade Federal da Bahia - Salvador (BA), Brazil, ZIP CODE: 40.170-110. E-mail: ibsilvacamara@hotmail.com, rodrigues.oliveira@hotmail.com, tatiana_geologia@yahoo.com.br, pedrorrsantana@gmail.com

(2) Grupo de Metalogênese, Centro de Pesquisa em Geofísica e Geologia - CPGG, Universidade Federal da Bahia, Salvador (BA), Brazil, ZIP CODE: 40.170-110. E-mail: aroldo.misi@gmail.com

(3) Programa de Pós-Graduação em Geociências e Análise de Bacias, São Cristóvão (SE), Brazil, ZIP CODE: 49100-000. E-mail: herbet@ufs.br

(4) Programa de Pós-Graduação em Geociências da Universidade Federal de Mato Grosso, Cuiabá (MT), Brazil, ZIP CODE: 78060-900. E-mail: pedrompgarcia@yahoo.com.br

Abstract

Brazil is the third biggest producer of graphite worldwide, with the state of Bahia being the second largest producer in the country, as most of the production comes from the Graphite Province of Bahia-Minas. The study area is situated at 350 km to the north of this producing region, in the Tanque Novo-Ipirá Complex, Itabuna-Salvador-Curaçá Orogen, São Francisco Craton. The area is comprised of host rocks with occurrences of graphite such as schists, marbles, and granulites as well as country rocks characterized by quartzites, calc-silicate rocks, marbles, and iron formations. The petrographic analysis supported by MEV/EDS indicates two generations of graphite: the first one, connected to the graphitization process generated by metamorphism (syngenetic), exhibit flakes with three distinct associations related to the greenschist, amphibolite, and granulite facies in which the host rocks were subjected; and the second generation, is related to the percolation of hydrothermal fluids (epigenetic) due to retrograde metamorphism in the

greenschist facies that promoted the deposition of graphite in venules or as a result of carbonation. The graphite bodies show a high total graphitic carbon (TGC), analyzed by LECO infrared, ranging from 8.70 to 15.98wt% and they occur in two distinct lithologies: aluminous and carbonate. The geochemical characteristics of the host and country rocks indicate sedimentary protoliths with signatures influenced by diagenetic alterations and detrital input in a marine paleoenvironment. However, they were not sufficient to change the anomalies of Ce/Ce* (0.64 to 1.49) that alongside the ratios of U/Th (0.04 to 1.30) suggest a paleoenvironment dominantly oxic. The analyzes of TGC with P/Ti, Ba/Ti, Ni and Cu show correlations that suggest the deposition of organic matter in a context of high organic paleo productivity. This depositional setting combining with the phosphorus anomalies in the country rocks, deposited during the Paleoproterozoic in an oxic paleoenvironment, suggest that the deposition of organic matter that originates the graphite might be related to the increase in paleo productivity generated following the Great Oxygenation Event (GOE), which culminated in the first major phosphogenesis event in the geological record.

Keywords: Graphite, total graphitic carbon, paleo productivity, Paleoproterozoic

1. INTRODUCTION

Graphite is a mineral characterized by its low hardness and density; it's highly refractory with a melting point over 3600°C, chemically inert, an excellent lubricant and it has the highest thermal and electric conductivity of non-metals. (Pierson 1993; Klein and Dutrow 2012; Jara et al. 2019).

Graphite ore is commercially classified into three types of deposits: vein (lump or chip), amorphous (microcrystalline graphite) and flake, with the world's largest producers being China, Brazil and India (Scherba et al. 2018). Average natural graphite production is estimated to be in the order of 1.0 to 1.2Mt per year, of this 600-800kt of flake graphite, 300kt of amorphous graphite and 4kt of vein graphite (Scogings 2019). Despite this natural graphite production, synthetic graphite accounts for about 90% of the market (Keeling 2017). A rapid increase in the price of the ore has been observed due to market speculation about graphene, but the main factors are: environmental regulations in China that have led to the closure of some mines and the increase in demand for graphite as anode in lithium batteries used in electric vehicles (Jara et al. 2019).

The state of Bahia, Brazil presents several graphite occurrences mapped by the Geological Service of Brazil (CPRM), with the Bahia-Minas Graphite Province being the largest graphite producing pole in Brazil (Pedrosa-Soares et al. 1999; Belem 2006). This province is located in the context of the Araçuaí Orogen, a Neoproterozoic belt that limits the southeastern edge of the São Francisco Craton (CSF), registering three mines in the towns of Maiquinique, Pedra Azul and Salto da Divisa. The fourth Brazilian mine is Paleoproterozoic and occurs in the southern CSF in the town of Itapecerica, correlated with deposits from the northern China Craton by Teixeira et al. (2017).

The occurrences analyzed in this work belong to the Tanque-Novo-Ipirá Complex (CTNI) and are located north of the graphitic Bahia-Minas Province (Figure 1). CTNI is a metavulcanosedimentary unit representative of a Paleoproterozoic basin integral of the Itabuna-Salvador-Curaçá Orogen, CSF (Kosin et al. 2003), which exhibits lithological association, graphite and phosphate mineralizations similar to those found in Kalahandi khondalite series, India (Walker 1902); Eastern Gates, Orissa, India (Dash et al, 1987; Bhattacharya et al. 2012); North China Craton (Ji et al. 1994; Zhong et al. 2019); Paraguayan Belt (Manoel and Leite 2018); and Ribeira Belt, Brazil (Pereira et al. 2016). The similarity of the CTNI to the khondalite complexes point to a high metallogenetic potential for graphite and phosphate.

This study represents a first characterization of the graphite mineralization at CTNI focusing on the description of the host and surrounding rocks of the mineralization. This characterization encompassed topics of basic geology, petrography and evaluation of the metamorphic grade of two CTNI graphite occurrences located at Morrinhos Farm and Serra do Camisão, which differ mainly in the degree of deformation and recrystallization. The geochemical characterization with interpretation of the degree of oxygenation and paleoenvironmental conditions was concentrated only on the occurrences of Morrinhos Farm due to the preservation of the primary signature. Finally, an initial genetic model was generated with the description of the metallogenetic processes forming the graphite deposit and its relationship with the phosphate occurrences of the bedrock, generating implications with the Great Oxygenation Event (GOE).
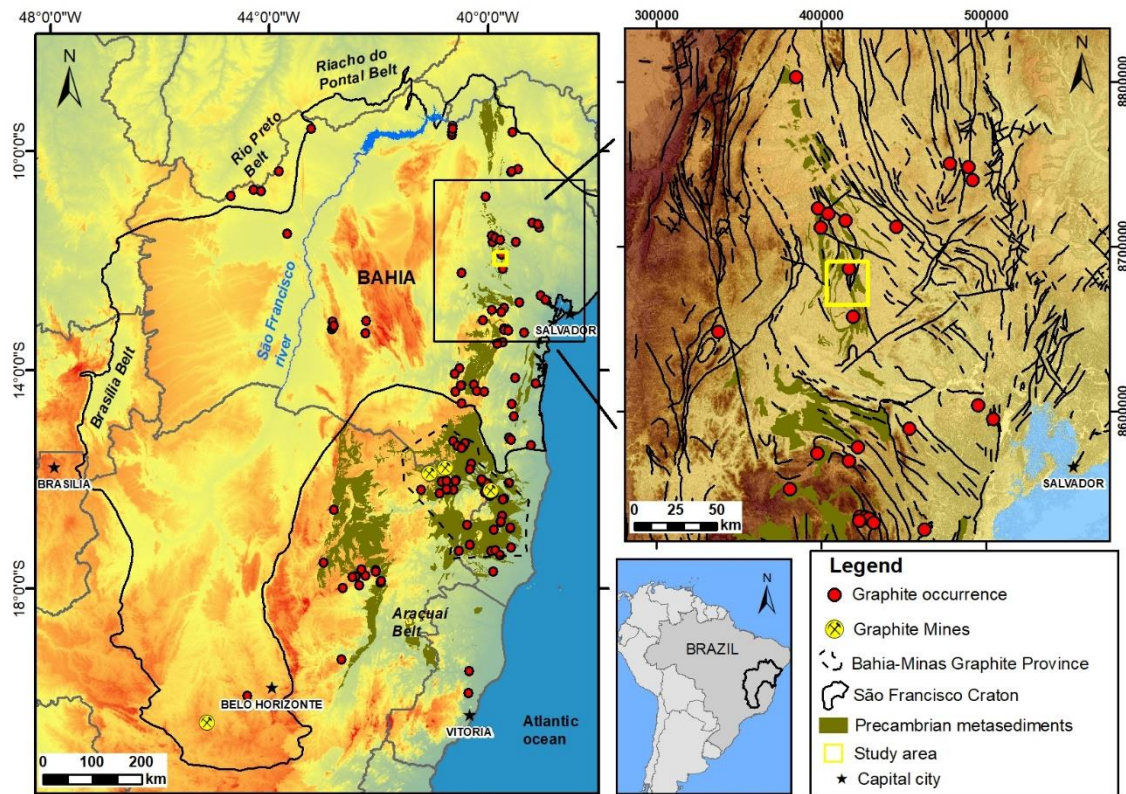
Figure 1: Location map of the study area in relation to the Bahia-Minas Graphitic Province. Source: Vector files, GeoSGB 2021.

2. REGIONAL GEOLOGICAL SETTING

The São Francisco Craton (CSF) corresponds to the crustal segment composed of Archean rocks and stabilized at the end of the Paleoproterozoic, Riacian-Orosirian periods, being limited by the orogenesis of the Brasiliano Cycle, between the Neoproterozoic and Cambrian (Almeida 1977; Alkmim et al. 1993). In the CSF stabilization event, the Gavião, Serrinha, Jequié and Itabuna-Salvador-Curaçá blocks collided, giving origin to the Itabuna-Salvador-Curaçá Orogen (OISC), an event that resulted in the emplacement of synchronic to post-tectonic granitoids and intrusion of mafic-ultramafic rocks (Barbosa and Sabaté 2004).

The northern region of the OISC, where the occurrences that are the object of this study are located (Figure 2A and 2B), is formed by three main lithostratigraphic units: (i) the Caraíba Complex, (ii) the São José do Jacuípe Suite (SSJJ), (iii) Tanque Novo-Ipirá Complex (CTNI), in addition to numerous Paleoproterozoic granitoid intrusions.

The CTNI represents the metavolcanosedimentary sequence and it is subdivided into 6 informal units by Kosin (1993), being composed mainly of quartzites, calcsilicate rocks, marbles, paragnaisses and graphite rocks. The U-Pb age obtained in detrital zircon

for the CTNI rocks indicate that this assemblage formed at least 2,128 Ma (Ribeiro et al. 2021).

This work focused on two occurrences of graphite at TNIC, the first located at Morrinhos Farm and the second at Serra do Camisão, this second is a region with greater interaction with granites and is known to have blue apatite mines (Figure 2C).
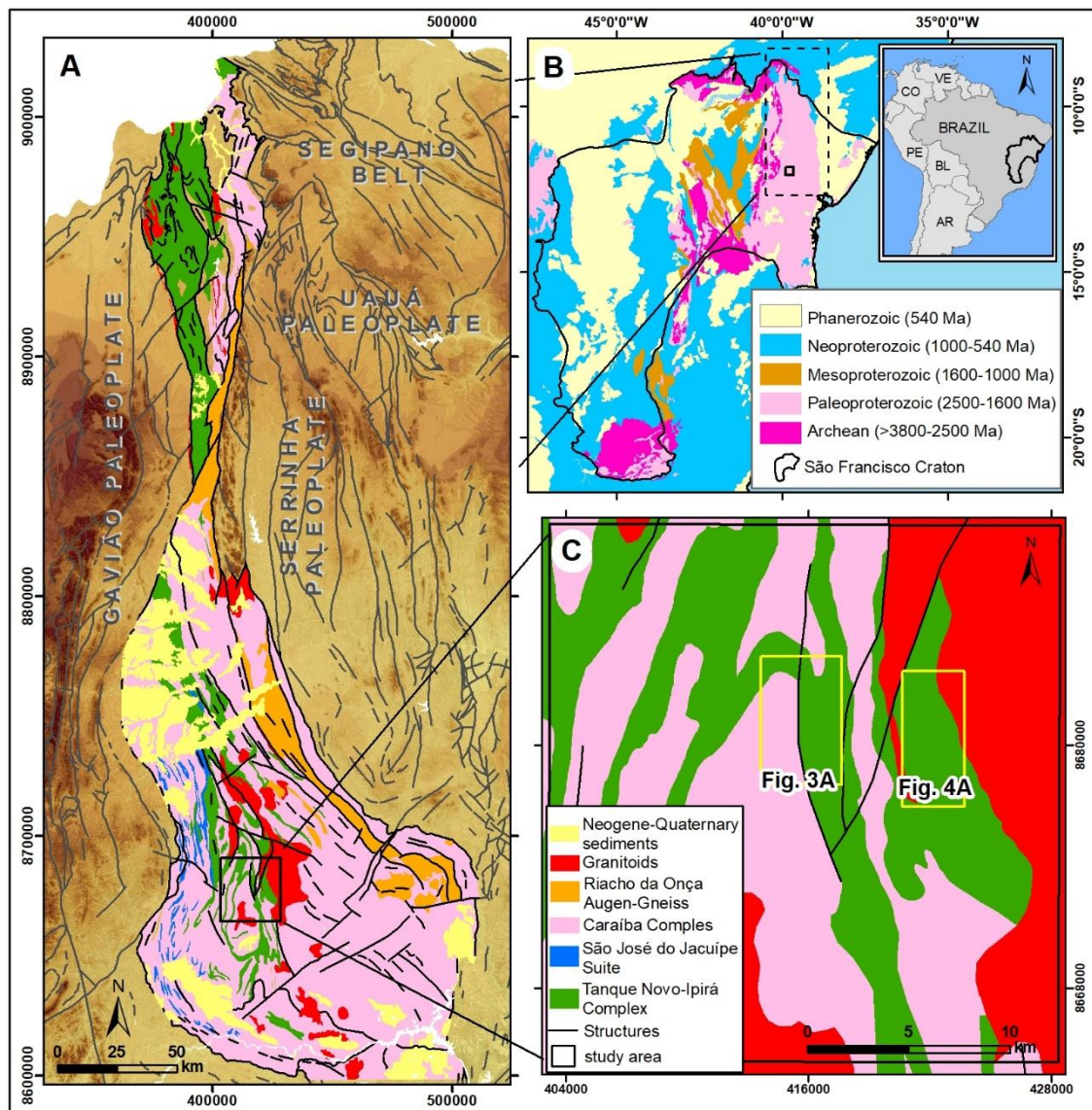

Figure 2: Geological setting and location of the study area. A. São Francisco Craton (SFC). B. Salvador-Curaçá Orogen member of the SFC, northeast of Brazil. C. Study area located in the Tanque Novo-Ipirá Complex, polygon A – the Morrinhos Farm, and B – the Serra do Camisão. Source: Vector files, GeoSGB 2021.

3. METHODOLOGY

3.1 Lithogeochemistry

The samples for the geochemical studies were prepared and analyzed in the SGS-Geosol laboratory. In total, 26 samples were analyzed: 13 graphite rocks, 5 calc-silicate rocks, 5 marbles, and 3 iron formation rocks. The analytical procedure involved particle size reduction of the samples by crushing 250g of rock.

The biggest elements (SiO_2, Ti_2O, Al_2O_3, MgO, Fe_2O_3t, MnO, CaO, Na_2O, K_2O, P_2O_5, and BaO) were measured using the technique of X-Ray fluorescence (FRX) by wavelength dispersion (WD). In this analysis, 0.5g of the samples were fully digested by fusion with lithium tetraborate at 1000ºC, creating the molten pearl. The analysis was performed on a WD-FRX, Axios FAST Model, obtaining results with a natural basis.

Trace elements (Rb, Ga, Zr, Sr, Cr, Ni, Co, and Y) and rare earth elements (REEs) were determined through digestion complete by fusion in a muffle at 950ºC with lithium metaborate ($LiBO_2$) and dissolved by acid solution with nitric acid and tartaric acid (HNO_3 and $C_4H_6O_6$). The trace elements were read by Inductively Coupled Plasma - Optical Emission Spectrometry (ICP-OES), model Optima 7300DV. That acid solution was also used to quantify rare earth elements that were read on a Nex Ion 300X model Mass Spectrometer (ICP-MS). ETR and Y (ETRY) concentrations were normalized using the average composition of the Post-Archean Australian Shale (PAAS) obtained by McLennan (1989);

Total Graphitic Carbon (TGC) and S analysis was preceded by a resistive combustion furnace, with oxygen gas, at a variable temperature of 2500ºC to 3000ºC, and infrared reading in LECO®. The values of C over 15% were reanalyzed with the prepared samples by acid digestion (HCl) and calcination in a muffle, and the carbon graphite was re-examined in LECO®.

3.2 Petrography and Scanning Electron Microscopy with Energy Dispersive Spectroscopy (SEM-EDS)

This analysis occurred in the Laboratory of Microanalysis of the Multiuser Geosciences Laboratory Complex at the Federal University of Sergipe (CLGeo-UFS). The Tescan Vega LMU3 scanning electron microscope (SEM) has attached secondary electron, backscattered electron, cathodoluminescence, and Energy Dispersive Spectroscopy (EDS) detectors from Oxford Instruments, model x-act.

The AZtecEnergy software was employed for automatic data acquisition, operating in the Quant subroutine. The energy spectra obtained was analyzed individually in order to eliminate the presence of false peaks, energy interference, and overlapping peaks. Moreover, the ZAF correction was used in the treatment of the chemical data. The EDS of the CLGeo is calibrated with copper's energy and the reliability degree of the analysis is evaluated based on the analysis of Astimex® international standards for silicates and oxides.

For SEM analysis, the thin-polished blades studied received a thin layer of carbon in order to optimize the readings. The analytical conditions in this study involved a voltage of 15kV and a current intensity ranging between 15 and 17nA, producing an electron beam with a diameter of 430nm. The average counting time was 60 seconds and the relative error was under 2% for most elements with oxide content greater than 10% by weight. Elements with concentrations below 5% exhibit an error from 4 to 19% and the detection limit of the spectrometer is 0.1% wt.

4. GEOLOGICAL CHARACTERIZATION OF GRAPHITE OCCURRENCES

The graphite bodies occur distributed among the Archean-Paleoproterozoic metavolcano-sedimentary rocks of the Tanque Novo-Ipirá Complex, mainly amid the counties of Ipirá and Pintadas. These bodies are elongated for about 4 km and have an apparent thickness varying from 60 to 5 meters, with an average of 20 meters. They follow the regional NNW foliation pattern, have a subvertical dip, and arise among the calc-silicate rocks (Figure 3A), marbles, quartzites and tremolites, interposed with lenses of paragnaisses (Figure 3B), iron formations, and chert. This lithological set is intruded by synchronic to late-tectonic granitoid bodies that exhibit pegmatite levels, milonitization features, augen-like structures and have generated metasedimentary alterations in the metasedimentary rocks.

The hosts of graphite occurrences are represented by schist (Figures 3C and 3D), marbles (Figure 3E) and gneiss (Figures 3F and 3G). These rocks occur folded, stretched generating the milonites or as lenses in granitoids (Figure 3H). Visually, graphite flakes vary according to the lithologies in which they are hosted, with the largest flakes being registered in the gneisses. The main alteration observed in these rocks is the formation of a ferruginous layer due to the oxidation of the material (Figure 3I).
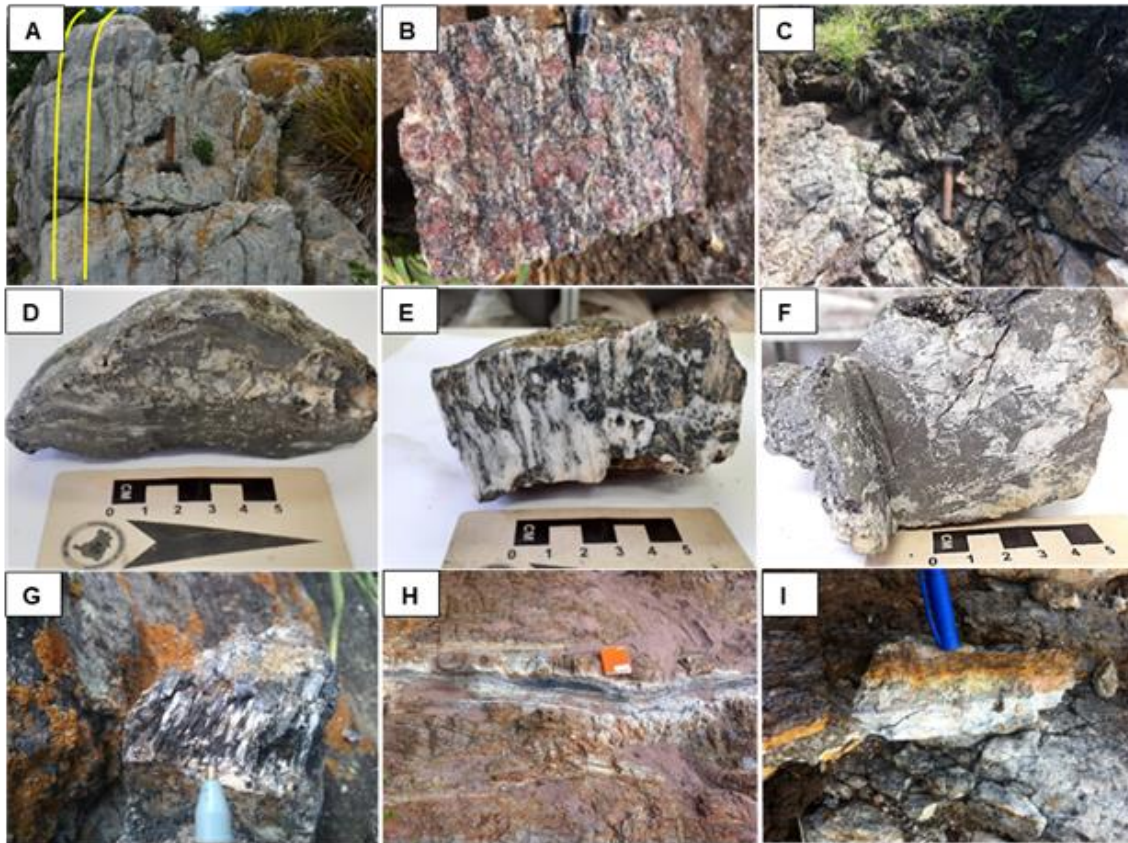
Figure 3: A. Calcissilicate outcrop showing the fold flank, close to the eroded hinge. B. Paragneisse sample. C. Fold in graphite schist, hammer is found in the hinge zone. D. Graphite schist with well-marked foliation. E. Graphite marble with carbonate venule cutting foliation. F. Sample of graphite gneiss. G. Graphite gneiss sample exhibiting large graphite flakes. H. Graphite lens between foliated granitoid. I. oxidized layer on graphite-shale.

4.1 Morrinhos Farm

At the Morrinhos Farm, the lithologies that host the mineralization correspond to graphite schist, graphite marble, and graphite ferruginous schist. The country rocks are comprised of olivine marble, quartzites, calc-silicate rocks, tremolitites, and diopsidites, being all intruded by granitoids (Figures 4A and 4B). The gradation between quartzites and calc-silicate rocks is subtle, and they are shown as a single unit in the map and cross section, whereas tremolites and diopsidites display halo alterations as a result of their interaction with granitic fluids from veins and granitoid bodies. Furthermore, occurrences of hydrothermal blue apatite in calciosilicates are also recorded.

The graphite flakes in the host lithologies present dimensions varying from 0.1 to 0.3 cm and in some outcrops it is possible to observe the formation of a ferruginous layer. Locally, graphite milonites generated from these lithologies are observed, with a

noticeable increase in the graphite content, but due to the milonitization process there is a recrystallization of the flakes.
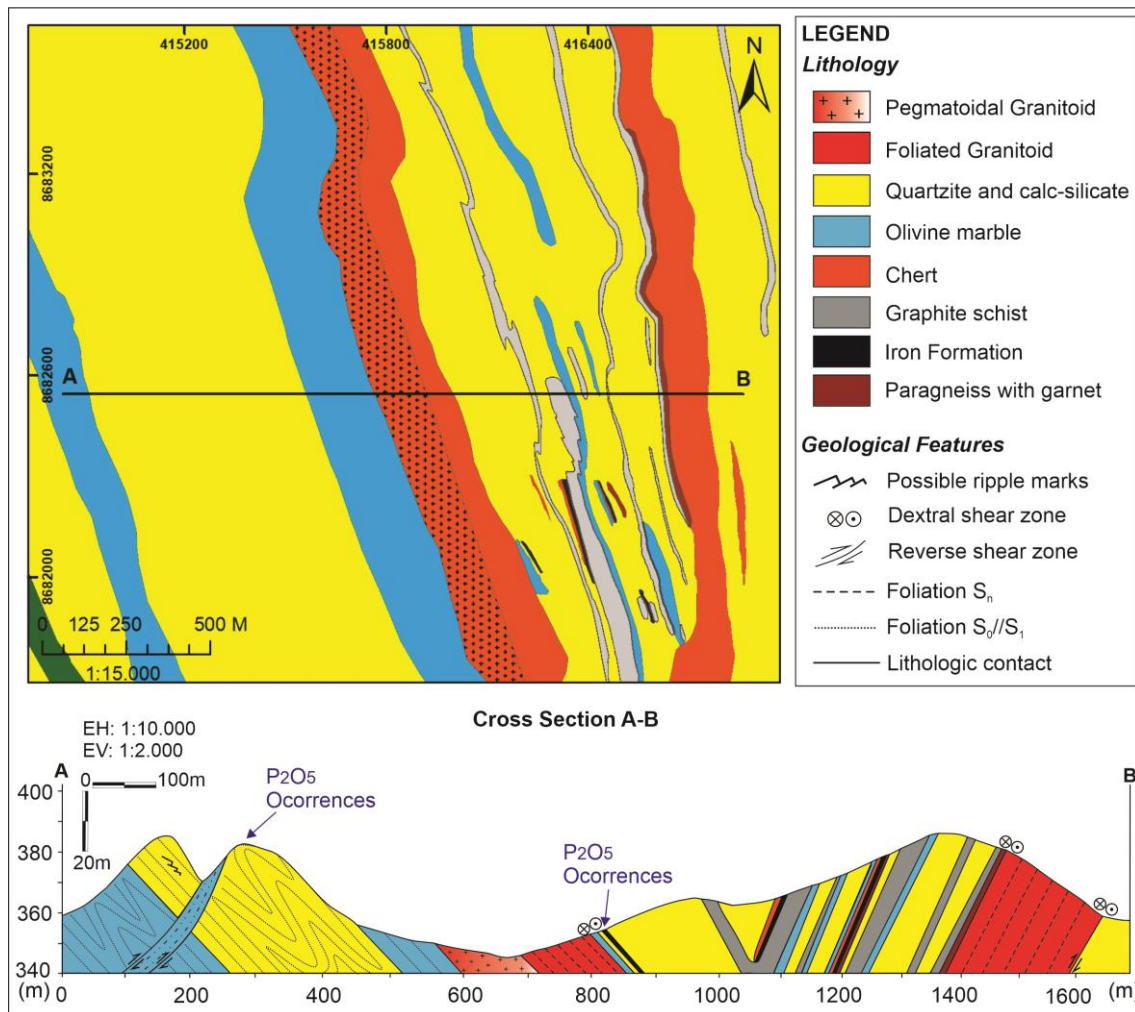
Figure 4: A. Geologic map of the Morrinhos Farm. B. Cross section A-B showing graphite levels, their country rocks, and phosphate ocurrences. Fonte: Author.

4.2 Serra do Camisão

Serra do Camisão is a region known for being home to several hydrothermal apatite mines originating from the interaction of metasedimentary rocks and granitoids. The graphite mineralization appears in the form of folded metasedimentary strata with an apparent thickness of 20 meters. The graphite mineralization occurs in the form of folded metasedimentary strata with an apparent uniform thickness of 20 meters. The host lithology of the graphite mineralization is represented by a graphitic gneiss and the underlying ones are marbles, calcsilicates and quartzites (Figures 5A and 5B). There are also protomilonites originating from these graphite bodies and graphite lenses about 5 to

20 cm thick embedded in foliated granitoids. In this location, the granitoid presents a strong influence, exhibiting levels of pegmatites that print a contact metamorphism on those metasedimentary rocks as well as metasomatism.
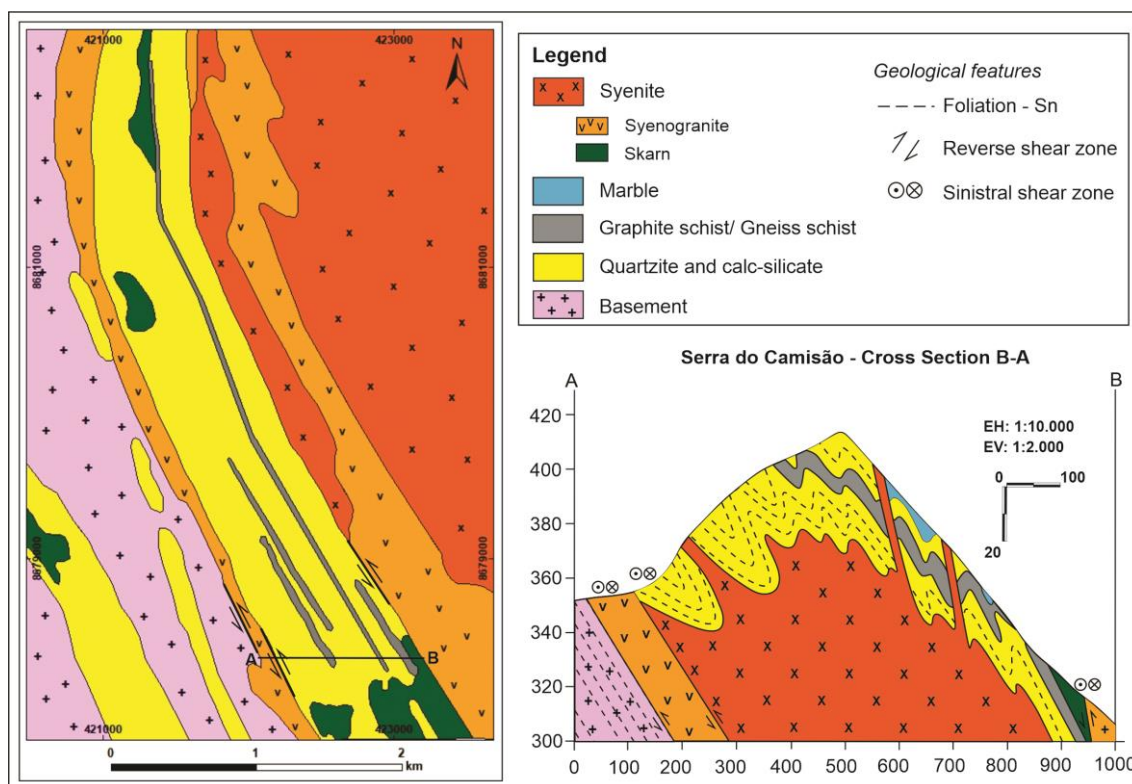
Figure 5: A. Geologic map of Serra do Camisão. Adapted from Melo et al. (1991). B. Cross section A-B showing graphite levels, their country rocks. Fonte: Author.

5. PETROLOGICAL ASPECTS OF MINERALIZATION HOST ROCKS

At the Morrinhos Farm, the host rocks of the graphite mineralization were named schists and graphite marbles, being petrographically classified as graphite-cordierite-actinolite schist, graphite-goethite-carbonate schist, hematite-graphite schist, graphite-cordierite marble, and serpentine-graphite marble. In the Serra do Camisão occurrence the graphite host rocks, more homogeneous, have been described only as graphite-chordierite granulite (Figures 6A, 6B and 6C).

The graphite schists are characterized by the orientation of graphite, biotite and muscovite with the development of a lepidoblastic and sheaf-like texture, gradating to granoblastic in places where there was a more intense recrystallization. Furthermore, it is observed two main trends in prismatic minerals (Figures 6A, 6B e 6C). The graphite has 106 to 3000µm of length, 50 to 600µm of thickness, and a modal estimation between 8

and 20%, being the minerals: quartz (40 to 50%); cordierite (5 to 15%), which is partially to completely pinitized in some places; muscovite (5 to 10%); biotite (2 to 10%); hornblende (2 to 8%); chlorite (2 to 6 %); diopside (2 to 5%); carbonates (0 to 5%); feldspar (0 a 4%); rutile (< 1%); titanite (< 1%); pyrite (< 1%); chalcopyrite (< 1%); baryte (< 1%); and apatite (< 1%). The supergenic minerals are comprised of iron oxide-hydroxide (1 to 12%); aluminous minerals of phosphate (< 1%); and clay minerals of the group of smectite (1 to 5%).

The graphite marbles from Morrinhos Farm exhibit massive to banded structures generated by the carbonates (Figures 6D, 6E e 6F). It has granoblastic texture displaying an incipient orientation, mainly from the graphite. The graphite contains granulometry between 50 and 1000μm, thickness varying from 20 to 600μm, and volume ranging from 7 to 25%. These large graphite flakes sometimes appear to be eroded by carbonate concordantly and also perpendicular to the foliation. These rocks correspond to diopsite-marble, where calcite/dolomite are predominant: calcite/dolomite (45 to 75%); diopside (15 to 22%); olivine (2 to 4%); garnet (1 to 3%); serpentine (2 to 20%); actinolite/tremolite (2 to 5%); hornblende (1 to 4%); epidote (1 to 5%); clay minerals (1 to 5%); muscovite (1 to 3%); and talc (1 to 3%). The accessory phases are: biotite (0 to 2%); goethite (0 to 2%); aluminous minerals of phosphate (< 2%); titanite (< 1%); sillimanite (< 1%); pyrite (< 1%); baryte (< 1%); chalcopyrite (< 1%); and galena (< 1%).

At Serra do Camisão the dominant lithology is graphite-cordierite gneiss presenting granoblastic, locally nematoblastic, porphyroblastic and sheaf textures generated by graphite and cordierite minerals (Figure 6G, 6H and 6I). In these gneisses the graphite crystals form large flakes with grain sizes in the range 106 to 7000 μm, thickness 20 to 2000 μm and volume varies from 15 to 25%, and occur in association with the minerals: quartz (40 to 55%); cordierite partially altered to pinite (8 to 12%); feldspar (5 to 10%); biotite (2 to 8%); epidote (2 to 6%); muscovite (2 to 5%); hypersthene (2 to 5%); hornblende (1 to 4%); chlorite (2 to 4%); hematite/goethite (1 to 4%); clay minerals (3 to 5%). And as the accessory phases are: pyrite (< 1%); chalcopyrite (< 1%); baryte (< 1%); titanite (< 1%); rutile (< 1%); apatite (< 1%); and phosphate (< 1%).
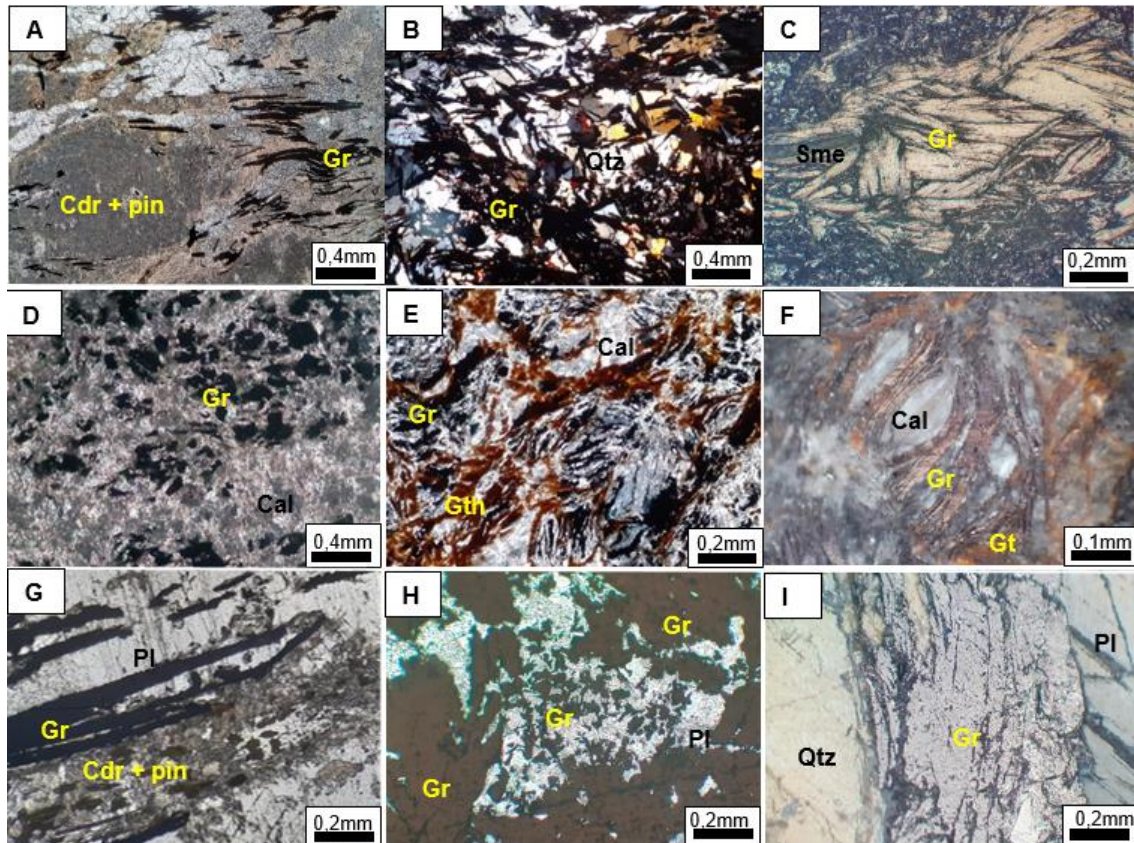
Figura 6: A. Pinitized cordierite porphyroblasts and flakes to large flakes (150-300 µm) of folded Gr. B. Flakes to large flakes of Gr in shale. C. Gr flakes with presence of Sme between the Gr sheets. D. Rounded Gr flakes in graphite marble E. Graphite marble with Fe enrichment F. Polished section exhibiting Cal between Gr sheets G. Graphite gneiss exhibiting large to super-jumbo flakes of Gr intergrown with pinitized cordierite H. Subidioblastic to xenoblastic large to jumbo flakes of Gr. I. Super-jumbo flake of idioblastic Gr in polished section. Calcite (Cal), cordierite (Cdr), goethite (Gth), graphite (Gr), pinite (pin), plagioclase (Pl), quartz (Qz), smectite (Sme) (Whitney and Evans, 2010).

The analyzed samples can be grouped into four metamorphic facies based on paragenesis and their corresponding metamorphic microtextures.

1. Granulite Facies

In the metapelites, the mineral assemblage in the granulite facies is characterized by Cpx (Hy), Grt, Cdr, Bt, Pl and Qz. The Cdr, Cpx (Hy) is a marker of the granulite facies and when associated with Grt it suggests high pressures.. In this association, fibrous inclusions of Sil in Pl and Cdr occurs.

In the granulite facies is attributed the crystallization of flakes (106-150 µm) to super-jumbo flakes (>500 µm) mainly in the graphite-chordierite granulite presenting idioblastics with tabular habits, straight edges, smooth textures, few inclusions and when it occurs is observed mainly among the lamellae: cordierite, quartz, plagioclase and in a secondary way micas and pyrite (Figures 7A and 8A). Graphite-associated pyrite occurs

in three distinct microtextures: the first as microcrystals and rounded shapes (<2.5 μm; Figure 7B). The second is characterized by straight edges and well-defined contacts (5 to 50 μm). The third occurs in aggregates with barite (<100 μm; Figure 7C).

2. Amphibolite Facies

In the graphite schist samples it is possible to notice the crystallization of hornblende on the edges of the pyroxenes that marks the amphibolite facies. While in the graphite marbles the diopside marks the upper limit of the amphibolite facies, actinolite and tremolite are minerals that indicate the lower amphibolite facies and are well marked on the edges of the diopside and hornblende crystals.

The flakes of graphite, attributed to the amphibolite facies, are observed mainly in schist rocks, marbles, and secondarily in the graphite-cordierite granulite. They form flakes (106–150μm) to jumbo flakes (300–500μm), both idioblastics, and also microcrystals (> 50μm) to jumbo flakes of subidioblastic graphite showing tabular habits, ragged to rounded edges, and smooth to botryoidal textures. Moreover, they present inclusions consisting mostly of micas, quartz, hornblende, actinolite/tremolite, carbonates, and secondary minerals corresponding to iron oxide-hydroxide and pyrite (Figures 7D and 8B).

3. Greenschist Facies

In the graphitic schists the index minerals of the green schist facies are muscovite, epidote, serpentine and chlorite. Whereas in the carbonate rocks those are serpentine, talc, calcite, dolomite, and quartz, originating mesh and curtain textures during the process of olivine's alteration.

It is also attributed to these facies the formation of microcrystals of graphite with rounded idioblastic to xenoblastic textures (<40μm), smooth to botryoidal textures, and inclusions of mica, Fe-rich carbonates, or siderite (Figure 7E). Graphite also occurs associated with veins and venules containing quartz, muscovite, calcite, barite, apatite, and sulfides with Au (Figures 7F and 7G).

4. Supergene alterations

The presence of clay minerals, primarily from the smectite and kaolinite groups, represents supergene alterations and/or low-temperature fluids, stimulating the oxidation and hydration of cordierite, besides the alteration of micas and serpentines. This

weathering alteration is well preserved nearby the regions with small graphite crystals or at the edges of the larger crystals (Figure 7H). It is also noticeable the formation of Fe oxides and/or hydroxides from sulfides and the production of secondary carbonates and phosphates (Figure 7I).
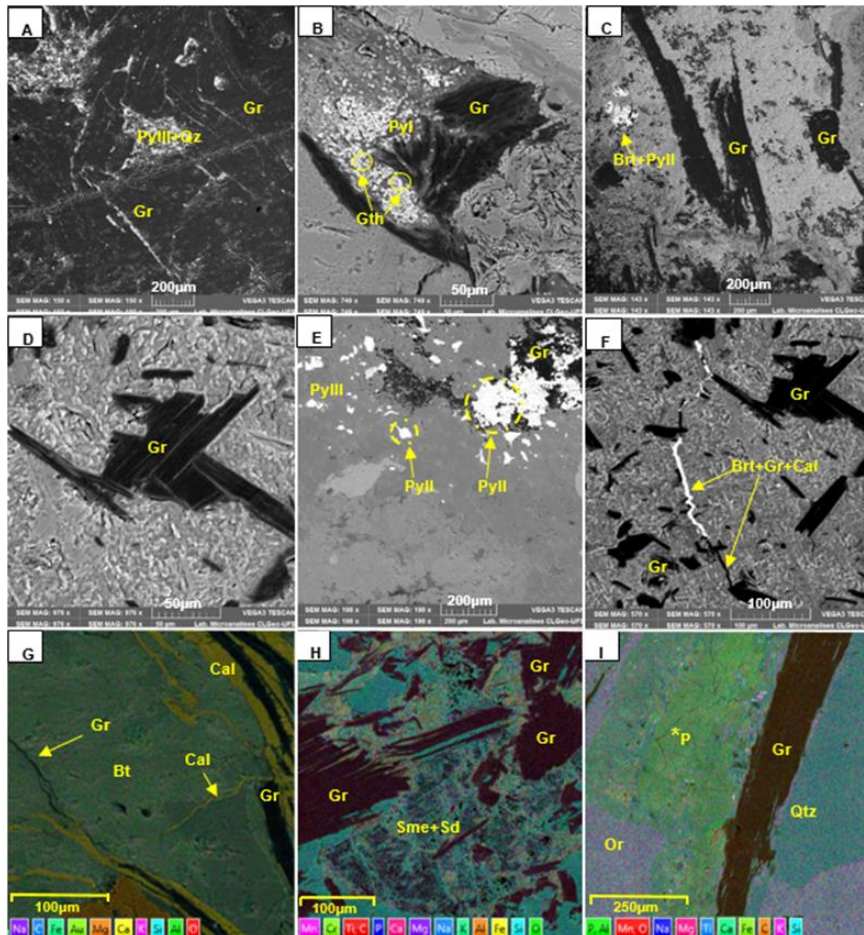
Figure 7: Electronic images obtained with a backscattering electron detector (BSE): A. Flakes to super-jumbo flakes of tabular graphite (Gr) with straight edges in granulite. B. Gr associated in granulite facies, note pyrite microcrystals and oxidized patterns of infilled framboids. C. Flakes to super-jumbo flakes of Gr with tabular, ragged, rounded edges and aggregates of barite and pyrite. D. Tabular Gr flakes with straight edges associated with amphibolite facies. E. Framboidal pyrite reliquites of filler or polybranched near microcrystals of Gr associated with shale-greenstone facies and metamorphic pyrites. F. Venules containing Brt, Gr and Cal; EDS element map showing: G. Venules containing impure Gr and Cal containing Mg and Fe concordant and transverse to foliation H. Microcrystals to Gr flakes with tabular and rounded edges near Sme and Sd. I. super-jumbo flakes of Gr in contact with secondary phosphate mineral (P). Barite (Brt), biotite (Bt), orthoclase (Or), pyrite (Py), and siderite (Sd) (Whitney and Evans 2010).
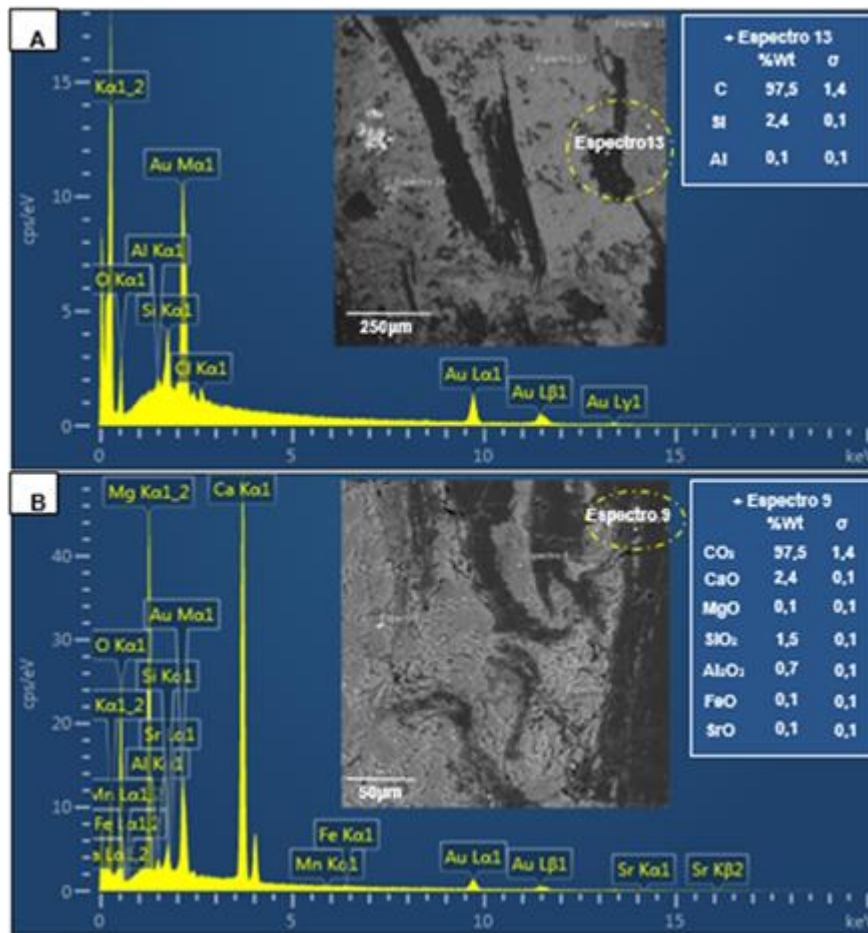
Figure 8. Diagram relating cps/eV (count per second by electron volts) versus keV (kilo electron volt) of minerals from the rocks studied. The images were obtained with a backscattered electron detector (BSE). The compositions of the minerals are presented (A) in percent cations and (B) percent by weight in oxides. The analytical error is indicated in the determinations and correspond to 1 sigma.

5.2 Lithogeochemistry

The results obtained for the biggest elements in the host rocks indicate two groups: aluminous, which correspond to graphitic schists and gneisses; and carbonatic, which correspond to graphitic marbles. SiO_2 varies from 53.71 to 72.83% in the aluminous host rocks and 7.41 to 33.23% in the carbonatic host rocks, while $CaO + MgO$ varies from 0.39 to 10.28% and 40.01 to 73.27%, respectively. The values in the aluminous and carbonatic hosts vary: TiO_2 (0.81 to 1.63%; and 0.28 to 1.03%), Na_2O (<0.1 to 1.19%; and <0.01 to 0.26) and K_2O (0.15 to 2.21%; and 0.07 to 1.19%), respectively, showing low values in both host rock groups. Al_2O_3 varies from 6.36 to 12.66% and Fe_2O_3 from 0.92 to 25.79% in the aluminous host rocks, while in the carbonatic host rocks Al_2O_3 varies from 1.37 to 8.59% and Fe_2O_3 varies from 0.32 to 2.34%. It is possible to observe in the aluminous host rocks that the S values vary from 0.02 to 0.16%, while in the carbonatic host rocks they vary from 0.02 to 0.26 %. High levels of graphitic carbon

occur, varying from 8.60% to 14.82% in the aluminous hosts and 10.77 to 15.98% in the carbonatic hosts.

Regarding the trace elements, Ni showed low values in the aluminous host rocks of 8.0 to 83.0ppm and in the carbonatic host rocks of <5.0 to 38.0ppm, while in the group of country rocks formed by calcisilicatics, marble and the iron formation there is a greater variation from <5.0 to 301.0 ppm. Furthermore, the content of Co is low in both host rocks, ranging from 1.0 to 12.4ppm in the aluminous group and from 0.9 to 18.4ppm in the carbonate group, whereas in the country rocks the content of Co ranges from 1.5 to 66ppm. Finally, the values of Cu in the aluminous host rocks fluctuate between 35.0 and 1246.0ppm, and it ranges from 27.9 to 112.0ppm in the carbonatic host rocks, whereas lower values (5.0 to 78.0ppm) are observed in the country rocks (Tables 2 and 3).

- Rare Earth Element and Yttrium (REY)

The sum of ΣETR ranges from 83.24 to 361.75 ppm in the aluminous rocks, 42.64 to 276.27 ppm in the carbonate rocks, and 5.90 to 375.70 ppm in the country rocks. The ETR values were normalized based on the PAAS (McLennan 1989) and it is noted that the aluminous hosts show a linear decreasing pattern indicating a slight enrichment of ETRL relative to ETRP, while the carbonatic hosts show a near flat pattern having a slight depletion relative to the normalizer (Figures 9A and 9B). In general, the country rocks present flat patterns, although it is possible to identify subtle hat shapes at the calc-silicate rocks and IF. Additionally, the country rocks show an overall depletion over the normalizer – PAAS, except for the IF and the IB-87 marble sample, which exhibit enrichment (Figures 9C and 9 D).

Negative Eu anomalies are well established in the host rocks, whereas the country rocks display slightly positive Eu anomalies, excluding some samples that exhibit high positive Eu anomalies (IB-11 and IB-39). Slight negative Ce anomalies are observed in both groups of host rocks and in most of the country rocks. Besides that, light negative Sm anomalies and positive Y anomalies appear in the calc-silicate rocks and marbles.

The Pr_N/Yb_N ratios vary from 0.66 to 3.25 and, in general, indicate enrichment of LREE over HREE in most of the host rocks, while there was an enrichment of HREE in most of the country rocks, with a variation in Pr_N/Yb_N ratios between 0.27 and 2.03. Sm_N/Pr_N. Ratios range from 0.92 to 1.18 in the host rocks and from 0.72 to 1.64 in the country rocks and these ratios basically indicate enrichment of MREE over LREE for most of the samples. In the host rocks, Sm_N/Yb_N ratios vary from 0.76 to 3.98 and in general denote an enrichment of MREE over HREE for most of the samples, whereas the

country rocks record a variation of 0.44 to 1.58 and most of these samples show HREE enrichment.

The calculations of the Eu/Eu*, Pr/Pr* and Ce/Ce* ratios reveal that the host rocks: present mostly negative Eu/Eu* anomalies (0.28 to 1.12), weak positive Pr/Pr* anomalies (1.03 to 1.12) and weak negative Ce/Ce* anomalies (0.64 to 0.98). The country rocks, on the other hand, present a predominance of positive Eu/Eu* anomalies (0.82 to 2.42), slightly positive Pr/Pr* anomalies (0.88 to 1.23), excluding the IB-46 marble sample; and a preponderance of negative Ce/Ce* anomalies (0.73 to 1.49).
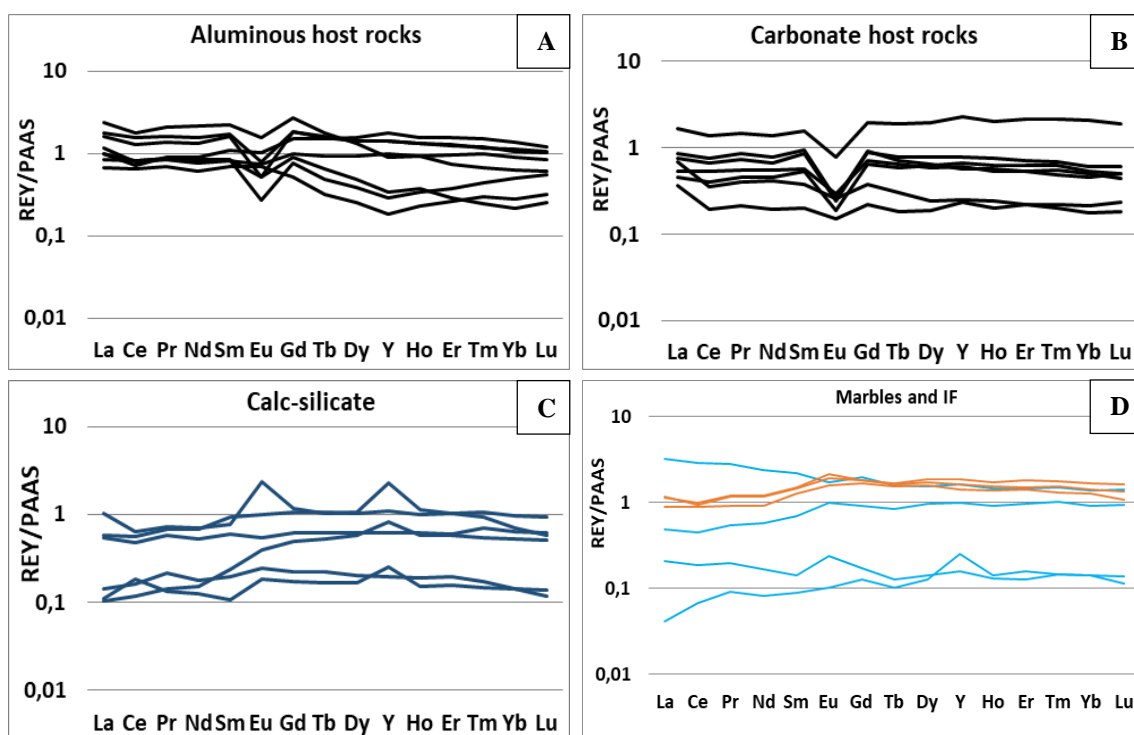

Figure 9: The ETRY pattern normalized by PAAS (McLennan, 1989): A. Aluminous host rocks. B. Carbonatic host rocks. C. Calc-silicate group of the country rocks. D. Marble and Iron formation, group of the country rocks.

Table 1: Lithogeochemical analyses of Total Graphitic Carbon (TGC), sulfur, major elements, and trace and rare earth elements of graphite host rocks.

Samples	IB-14	IB-14B	IB-19A	IB-19B	IB-20A	IB-20B	IB-24A	IB-24B	IB-28A	IB-28B	IB-35	IB-54	IB-TA
	Schist	Schist	Schist	Marble	Schist	Schist	Marble	Marble	Schist	Schist	Marble	Marble	Marble
C (wt%)	13.19	14.82	8.60	15.83	12.29	9.38	13.89	15.98	-	12.86	10.77	11.89	15.87
S	0.02	0.04	0.02	0.04	0.02	0.16	0.04	0.26	-	0.03	0.04	0.02	0.06
SiO_2	67.53	71.64	64.46	23.44	72.83	53.71	33.23	14.56	-	55.45	29.56	7.41	21.52
TiO_2	1.63	1.44	1.01	0.28	1.10	0.81	0.43	0.48	-	1.02	1.03	0.67	0.44
Al_2O_3	12.66	6.36	12.28	3.92	9.21	7.60	5.54	5.86	-	6.79	8.59	3.96	1.37
Fe_2O_3	0.92	0.95	1.50	0.38	1.85	25.79	0.82	0.32	-	18.65	2.34	1.46	0.77
MnO	0.02	0.05	0.03	<0.01	0.02	0.08	<0.01	<0.01	-	0.01	0.03	<0.01	<0.01
MgO	0.55	0.32	4.40	18.41	0.27	0.18	17.01	20.10	-	0.41	13.63	28.91	17.55
CaO	0.28	0.62	5.88	27.62	0.20	0.21	23.00	32.98	-	0.23	31.32	44.36	30.49
Na_2O	0.13	0.25	0.00	0.15	0.11	<0.01	0.20	0.00	-	0.13	0.26	<0.01	0.15
K2O	1.18	0.85	0.20	0.79	0.15	0.18	1.29	1.29	-	1.89	0.96	0.07	0.22
P_2O_5	0.09	0.05	0.06	<0.01	0.04	0.69	0.57	0.01	-	0.05	0.01	0.05	1.41
BaO	<0.01	0.09	0.05	0.05	<0.01	<0.01	0.17	0.06	-	0.08	0.07	<0.01	0.26
Total	98.20	97.50	98.50	90.90	98.10	98.80	96.20	91.90	-	97.60	98.60	98.80	90.10
Rb (ppm)	15.6	15.0	20.0	5.1	5.2	2.4	19.2	32.3	108.7	75.3	27.2	2.2	0.8
Ga	17.7	30.1	6.8	22.6	20.2	11.0	7.9	8.2	41.8	18.7	11.6	4.9	3.8

Mo	3.0	2.0	3.0	53.0	6.0	6.0	2.0	2.0	8.0	5.0	2.0	3.0	2.0
Ni	22.0	36.0	8.0	37.0	83.0	79.0	<5	9.0	27.0	17.0	30.0	38.0	21.0
Co	2.0	2.4	1.0	18.4	8.3	12.4	1.5	0.9	3.9	1.2	5.6	2.4	2.0
Cu	1246.0	35.0	73.0	112.0	137.0	256.0	78.0	27.0	47.0	40.0	58.0	79.0	29.0
Th	14.8	17.2	14.0	5.0	14.4	6.7	6.0	7.4	25.0	19.0	9.2	1.7	3.8
U	2.1	2.7	0.9	2.8	3.3	1.8	1.0	1.3	2.5	1.8	1.4	0.5	0.7
Y	38.3	24.5	18.2	61.2	37.6	26.8	16.3	20.9	7.8	5.0	15.5	6.2	6.7
La	68.4	90.4	17.6	62.7	60.9	44.2	20.4	28.7	31.8	25.8	32.5	14.0	26.4
Ce	124.2	140.6	32.2	108.6	101.6	62.0	42.5	53.2	63.9	51.4	60.2	15.2	27.7
Pr	14.3	18.3	4.1	13.0	11.9	7.5	4.9	6.5	7.7	6.1	7.5	1.9	3.5
Nd	52.8	73.3	15.4	46.9	45.3	25.5	18.5	22.8	27.7	20.5	26.3	6.6	14.2
Sm	9.4	12.2	3.0	8.8	8.8	4.5	3.2	4.8	4.6	3.9	5.3	1.1	2.1
Eu	0.8	1.7	0.2	0.8	0.6	0.8	0.3	0.3	0.3	0.2	0.3	0.2	0.3
Gd	8.7	12.4	3.0	9.2	8.5	4.6	3.3	4.1	3.6	2.4	4.3	1.0	1.8
Tb	1.3	1.4	0.5	1.5	1.2	0.7	0.5	0.6	0.4	0.3	0.5	0.1	0.2
Dy	6.6	6.1	2.9	9.1	6.7	4.3	2.7	3.7	1.8	1.2	3.0	0.9	1.1
Ho	1.3	0.9	0.6	2.0	1.3	0.9	0.5	0.8	0.3	0.2	0.6	0.2	0.2
Er	3.6	2.1	1.8	6.1	3.6	2.7	1.5	2.0	1.1	0.7	1.5	0.6	0.6
Tm	0.5	0.3	0.3	0.9	0.5	0.4	0.2	0.3	0.2	0.1	0.2	0.1	0.1
Yb	3.0	1.8	1.5	5.9	3.2	2.5	1.4	1.7	1.4	0.8	1.3	0.6	0.5
Lu	0.4	0.3	0.2	0.8	0.5	0.4	0.2	0.3	0.2	0.1	0.2	0.2	0.4
ΣETR	295.3	361.8	83.2	276.3	254.5	161.1	100.1	129.7	144.9	113.8	143.6	42.6	78.9
ΣLREE	259.7	322.6	69.3	231.2	219.7	139.2	86.3	111.2	131.1	103.8	126.5	37.7	71.8
ΣHREE	15.4	11.5	7.3	24.8	15.7	11.3	6.6	8.7	5.0	3.2	6.8	2.5	2.7
ΣLREE/ ΣHREE	16.8	28.1	9.5	9.3	14.0	12.4	13.1	12.8	26.0	32.3	18.6	15.1	27.0
Ce/Ce*	0.9	0.8	0.9	0.9	0.9	0.8	1.0	0.9	0.9	0.9	0.9	0.7	0.6
Pr/Pr*	1.0	1.1	1.1	1.1	1.0	1.1	1.0	1.1	1.1	1.1	1.1	1.1	1.0
Eu/Eu*	0.4	0.6	0.4	0.3	0.3	0.8	0.5	0.3	0.3	1.1	0.3	0.7	0.7
Pr_N/Yb_N	1.5	3.2	0.7	0.9	1.2	1.0	1.1	1.2	1.7	2.4	1.8	1.0	2.3
Sm_N/Pr_N	1.04	1.06	1.18	1.08	1.18	0.96	1.04	1.17	0.96	1.02	1.13	0.92	0.95
Sm_N/Yb_N	1.59	3.44	1.02	0.76	1.40	0.91	1.16	1.43	1.67	2.48	2.07	0.93	2.13

Table 2: Analyses of trace and rare earth elements of the country rocks.

Samples	IB-11	IB22A	IB-32	IB-39	IB-41A	IB-41B	IB-46	IB-47A	IB-49A	IB-56C	IB-65A	IB-87	IB-88
	Calc	Calc	IF	Marble	Marble	Marble	Marble	IF	Calc	IF	Calc	Marble	Calc
Rb (ppm)	15.2	2.6	6	0.9	35.5	0.8	0.6	1	11.1	1.9	25.4	1.2	3.8
Ga	2.4	14.4	17.9	2.4	20.7	0.8	2.4	12.3	4.8	15.4	17.3	0.1	2.8
Zr	116	105	159	27	120	12	33	143	138	142	39	16	46
Sr	149	32	75	49	93	44	50	82	32	29	195	241	23
Mo	4	5	4	3	3	3	3	5	3	26	6	4	4
Ni	43	301	171	35	57	9	11	137	17	200	114	33	5
Co	5.2	35.1	62.4	5.7	20.1	4.1	4	57.5	7	65.3	18.3	6.3	4.1
Cu	8	5	8	13	14	13	13	11	8	9	6	53	8
Th	13.6	4.2	9.6	0.4	3.8	<0.1	0.2	8.7	11.8	9.4	4.2	9.1	7.6
U	0.84	0.5	3.09	0.27	3.53	0.13	0.24	3.89	3.07	3.06	2.02	0.37	0.91
Y	61.94	21.98	50.3	4.33	26.73	6.86	6.83	38.44	16.42	44.43	29.28	43.93	5.34
La	39.6	3.9	43.3	7.9	18.9	1.6	4.2	33.8	20.9	45.2	21.9	124.3	5.4
Ce	50.8	9.3	79.4	15	36.2	5.4	14.5	70.5	38.2	75.7	44	228.1	13
Pr	6.34	1.26	10.79	1.77	4.83	0.82	1.19	8.19	5.09	10.39	5.94	24.81	1.87
Nd	23.6	5.1	41.4	5.7	19.3	2.8	4.2	31.2	17.6	39.8	22.9	80.6	6.1
Sm	4.3	1.3	8.3	0.7	3.9	0.2	0.6	7	3.3	8.1	5.1	12.1	1.1
Eu	2.52	0.43	2.34	0.26	1.07	0.11	0.2	1.73	0.59	2.1	1.08	1.84	0.26
Gd	5.37	2.27	8.38	0.8	4.33	0.59	0.79	7.72	2.86	8.5	4.99	9.17	1.02
Tb	0.79	0.4	1.31	0.1	0.66	0.08	0.13	1.2	0.48	1.27	0.81	1.24	0.17
Dy	4.9	2.69	8.3	0.67	4.49	0.6	0.79	7.45	2.89	8.01	4.84	7.14	0.95
Ho	1.11	0.58	1.7	0.13	0.9	0.14	0.15	1.37	0.61	1.53	0.97	1.45	0.19
Er	2.92	1.65	5.18	0.36	2.74	0.45	0.44	4	1.72	4.28	2.89	4.12	0.55
Tm	0.38	0.22	0.71	0.06	0.41	0.06	0.06	0.53	0.28	0.62	0.43	0.61	0.07
Yb	2	1.5	4.7	0.4	2.6	0.3	0.4	3.6	1.8	4	2.7	3.9	0.4
Lu	0.25	0.22	0.7	0.05	0.41	0.05	0.05	0.47	0.27	0.59	0.41	0.62	0.06
ΣETR	144.88	30.82	216.88	34	100.74	13.61	27.7	178.76	96.59	210.09	118.96	500	31.14
ΣLREE	127.16	21.29	185.53	31.33	84.2	10.93	24.89	152.42	85.68	181.29	100.92	471.75	27.73
ΣHREE	17.72	9.53	31.35	2.57	16.54	2.27	2.81	26.34	10.91	28.8	18.04	28.25	3.41
ΣLREE/ ΣHREE	7.18	2.23	5.92	12.19	5.09	4.81	8.86	5.79	7.85	6.29	5.59	16.70	8.13
Ce/Ce*	0.73	0.95	0.85	0.92	0.87	1.00	1.49	0.98	0.85	0.81	0.89	0.95	0.92
Pr/Pr*	1.08	1.07	1.10	1.12	1.07	1.23	0.88	1.03	1.15	1.11	1.10	1.07	1.23
Eu/Eu*	2.42	2.10	1.32	1.52	1.21	0.94	1.33	1.10	0.90	1.18	1.01	0.82	1.15
Pr_N/Yb_N	1.01	0.27	0.73	1.41	0.59	0.65	0.95	0.73	0.90	0.83	0.70	2.03	1.49
Sm_N/Pr_N	1.08	1.64	1.22	0.72	1.28	0.97	0.80	1.36	1.03	1.24	1.37	0.78	0.94
Sm_N/Yb_N	1.09	0.44	0.90	1.02	0.76	0.63	0.76	0.99	0.93	1.03	0.96	1.58	1.40

6. DISCUSSION

6.1 Metamorphism

The graphitization process is irreversible and a direct function of the metamorphic temperature, with little to no influence of pressure (Luque et al. 1998; Aoya et al. 2010).

Therefore, it becomes possible to associate graphitization with metamorphic evolution, with three regressive metamorphic facies being clearly marked in the samples, ranging from granulite to greenschist.

In the aluminous host rocks, the peak metamorphic assemblage attributed to the granulite facies is characterized by Opx (Hy), Cdr, Grt, Bt, Pl, and Qz. These mineral associations in the host rocks and calc-silicate rocks indicate metamorphic temperatures of the order of 700°C (Bucher and Grapes 2011), to which are attributed the entire ordering of the graphite crystal (Pasteris and Wopenka 1991). In graphite hosts, the crystallization of flakes (106–150 μm) to super-jumbo flakes (>500 μm) of graphite idioblasts is attributed to the granulite facies.

The superposition of events during orogenesis makes it difficult to distinguish the progressive/regressive amphibolite and green schist facies, especially when trying to associate the crystallization of graphite. Therefore, it was possible to attribute to the amphibolite facies regressive metamorphism, the crystallization of microcrystals (> 50 μm) to jumbo flakes (300–500 μm) of graphite with idioblastic to subidioblastic habits, as the graphitization process is irreversible and records the last temperature metamorphic that made possible the rearrangement of the graphite crystal. Finally, there is the relaxation phase of the Salvador-Curaçá orogen with percolation of fluids under greenschist facies conditions and crystallization of graphite microcrystals (<40 μm).

There are relict textures in pyrites, occurring as pyrite microcrystals (<2.5 μm), in rounded shapes that suggest filling fambrids (10 μm) or poly-fambroid aggregates (<100 μm), it can also be associated with this group the aggregates of pyrite and barite (<100 μm). The relict pyrites are distinguished from metamorphic pyrites because that last have straight edges and well-defined contacts (5 to 50 μm).

The metamorphic evolution is registered in the samples by a granulite facies peak and a retrograde metamorphism from amphibolite facies to greenschist, having in the final events of the orogeny been registered the percolation of hydrothermal fluids. Based on the information presented of the petrographic analysis, there are two types of graphite can be classified as the syngenetic and epigenetic.

The first is associated with the process of graphitization generated during the progressive metamorphism and stabilized in regressive metamorphism, which occurs in most of the samples, and can be characterized as syngenetic with three distinct associations that vary with the metamorphic facies: granulite, amphibolite and
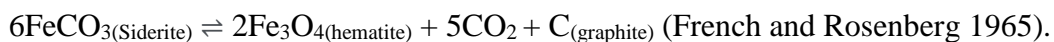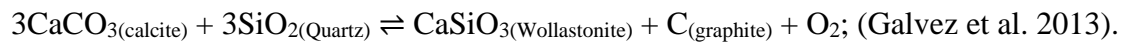
greenschist. The graphitization reaction can be synthesized in a simple way, according to Busseck and Beyssac (2014):

$$\text{C-H-O-N-S (}_{\text{Organic molecules}}) \rightarrow \text{Pure Carbon (}_{\text{Graphite}})$$
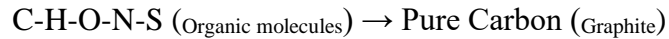
The second typology is of the epigenetic type, attributed to percolation of hydrothermal fluids and deposition of graphite in veins and venules, occurring secondarily in the samples. The reactions below are referred to graphite deposition from fluids, according to Kwiecińska and Petersen (2004):

$$2CO \rightarrow C_{\text{(graphite)}} + CO_2$$

$$2CO + 2\,H_2O \rightarrow 2CO_2 + 2H_2 \rightarrow C_{\text{(graphite)}} + 2H_2O$$
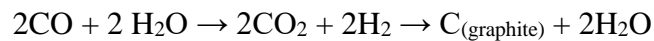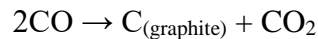
Also, in relation to epigenetic graphite, it is noted that reactions with hydrothermal fluids rich in Ca-C-Fe-Ba-S, recorded by carbonate, graphite, sulfate, and sulfide venules, generate destabilization of syngeneic graphite, which is marked by the presence of eroded edges, lower grain size, vermicular and botyroidal habits. Some retrograde reactions to destabilize clinopyroxenes and Fe oxides can be attributed to this corrosion in graphite, being:

$$3CaCO_{3\text{(calcite)}} + 3SiO_{2\text{(Quartz)}} \rightleftharpoons CaSiO_{3\text{(Wollastonite)}} + C_{\text{(graphite)}} + O_2; \text{ (Galvez et al. 2013).}$$

$$6FeCO_{3\text{(Siderite)}} \rightleftharpoons 2Fe_3O_{4\text{(hematite)}} + 5CO_2 + C_{\text{(graphite)}} \text{ (French and Rosenberg 1965).}$$

6.2 Protoliths and Material Source

The country and host rocks have low Ni values when compared to primary magmas that have a variation of Ni between 400 and 500ppm (Winter 2009). They also have low Co values in comparison with ultramafic rocks that have an average of 150 ppm of Co (Fleisher and Parker 1967). These results suggest a sedimentary origin of the protoliths.

On the diagram developed by Simonen (1953), the carbonatic host rocks are plotted in the field of calcareous sedimentary rocks, whereas the aluminous host rocks are plotted in the fields of pelitic and arenaceous rocks (Figure 10A). On the other hand, on the diagram developed by Herron (1988), the carbonate and aluminous host rocks are distributed in the fields of arkose, ferruginous sandstones, and shales (Figure 10B). On the Th vs. K diagram (Schlumberger 2009), which discriminates clay minerals, the aluminous and carbonate host rocks are plotted close to the field of chlorite, montmorillonite and heavy minerals containing Th.

This variation in composition suggests a mixture of clay minerals and expresses the influence of detrital minerals containing Th, verified by the presence of thorite in

petrography (Figure 10C). The TiO2 vs. Ni diagram (Floyd et al. 1989) indicates the provenance from acid rocks and magmatogenic greywackes for the protoliths of the aluminous host rocks and from acid rocks for the protoliths of the carbonate host rocks. It suggests a predominantly acid basement as well as immature sediments as the source material of the metasediments (Figure 10D).
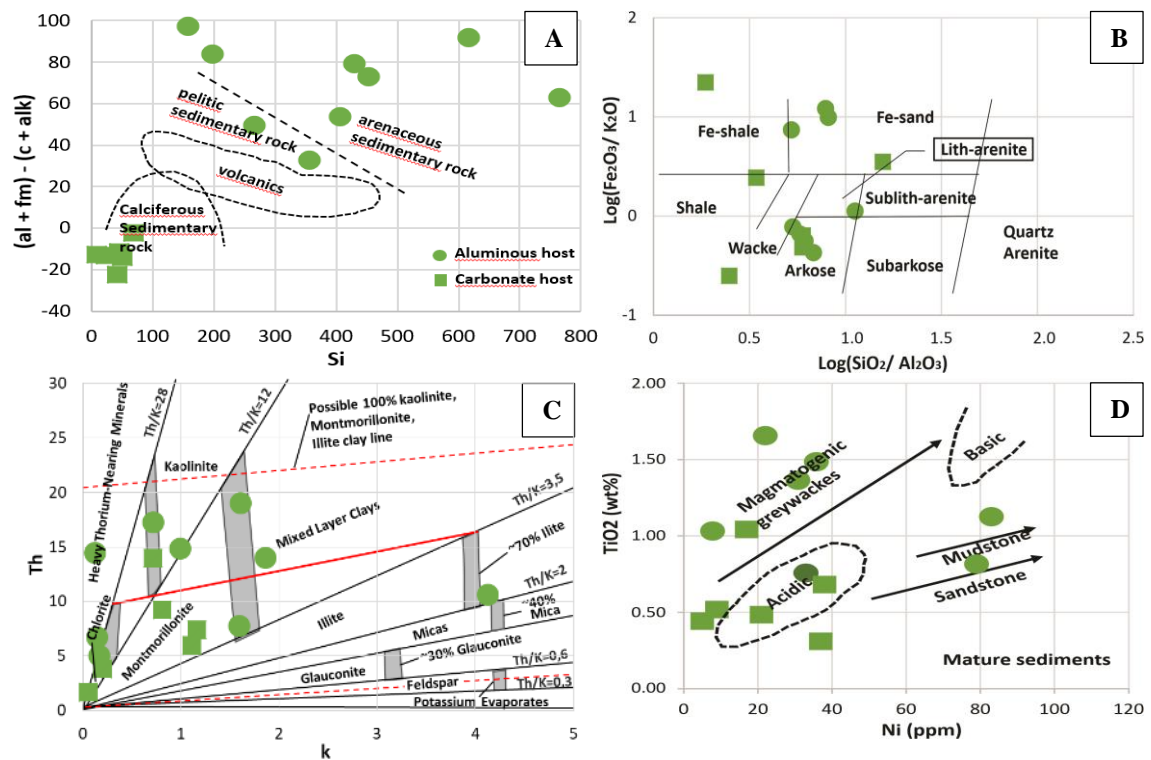

Figure 10: A. Diagram (al + fm)-(c + alk) versus Si for the hosts (Simonen 1953). B. Geochemical classification and discrimination of the analyzed rocks using the log (SiO2/Al2O3) versus log(Fe2O3/K2O) system of Herron (1988). C. Classicization of clay minerals according to K versus Th contents (Schlumberger 2009). D. Ni versus TiO2 diagram indicating sources of acidic rocks and magmatogenic grauvases (Floyd et al. 1989). Caption: green circles indicate aluminous hosts and green squares carbonate hosts.

6.3 Paleoenvironmental Conditions

In the analysis of metasediments, the investigation of paleoenvironmental conditions can be traced through the interpretation of the ETRY patterns that show relative immobility in secondary geological processes. For this purpose, it is necessary to evaluate the detrital contribution; the alteration degree of the primary signature, generated by changes during post-depositional processes as diagenetic effects (Shields and Stille 2001; Bolhar and Van Kranendonk 2007); and the alteration provoked by metamorphic and hydrothermal fluids (Bau and Dulski 1996; Alexander et al. 2008).

Chemical sediments have the propensity to preserve, more consistently, the geochemical signature at the time of deposition than detrital sediments (Bau and Dulski 1996). Ribeiro (2021) performed a lithogeochemical survey of the TNIC focusing on the paleoenvironmental reconstruction and the description of the processes involved in phosphogenesis in marbles and calc-silicate rocks. In order to locally observe some variation of the pattern analyzed by the aforementioned authors and seeking to verify its relationship with the aluminous and carbonatic hosts, the group of the surrounding areas was analyzed: calcisilicates, marbles, and iron formations.

The Y/Ho ratio was applied to verify the presence of detrital components within a basin in which an open marine environment is indicated by the Y/Ho ratio ranging from 40 to 80, whereas lower ratios (33 to 40) denote coastal or lagoon environments (Bau et al 1997; Nozaki et al. 1997), and continental water bodies present a ratio close to PAAS values of 27 (Tostevin et al. 2016). The Y/Ho ratios of the host rocks range from 21.65 to 31.38, whereas in the country rocks these ratios are higher and vary from 26.92 to 55.80. Considering that the metamorphic and diagenetic processes have a low influence on the primary signature of the Y/Ho ratio (Bau 1999), the samples plotted in Figure 11A suggest a higher marine contribution for the source rocks, while for the host rocks there is a higher detrital contribution with values close to the PAAS.

The enrichment of Eu and La may be indicative of diagenetic alteration and/or contribution of hydrothermal fluids in the seawater originating from fumaroles associated with MORB-like volcanic rocks during the deposition of sediments in the paleobasin (Khelen et al. 2019). The positive correlation between Eu/Eu $*$ and Pr/Sm_N observed in Figure 11B infers that the Eu was not dissociated from ETRY in redox reactions during diagenesis (Bolhar and Van Kranendok 2007), neglecting the IB-11 sample since it presented Ba/Nd > 145, which is suggestive of Ba interference in Eu values during the analysis by ICP (Dulski, 1994). The analysis of Figure 8C evaluates the influence of fumarole fluids in the metasediments, showing that the samples exhibit a positive correlation between ΣREE vs. La and minor dispersion between the samples of each group that suggests, consequently, a low influence of fumarole fluids (Manikyamba et al. 1993; Khelen et al. 2019).

The ratios of Eu/Sm vs. Y/Ho and Sm/Yb mark compositions of mixtures of seawater with hydrothermal fluids (Klein and Beukes 1989; Khan et al. 1996). The model proposed by Alexander et al. (2008) indicates that an influence <1% of hydrothermal fluids in Archean sediments does not significantly alter the geochemical signature of the

rocks. In Figures 11D and 11E, the country rocks, mainly calc-silicates and marbles, are plotted closer to the field of seawater while the host rocks are plotted in the field of sediments studied by Ribeiro (2021).

The Sm_N/Yb_N ratios are used to identify the fractionation between MREE and HREE, whereas the Sm_N/Pr_N ratios identify the fractionation in MREE and LREE. In Figure 11F, most of the host and country rocks are plotted close to the central region of the graph. It indicates a low fractionation for these samples, but with an overall enrichment in LREE and MREE suggesting the influence of diagenetic changes in the samples and/or detrital contamination (Reynard et al. 1999; Samala et al. 2018). Some aluminous host rocks (IB-19B and IB-79), calc-silicate rocks (IB-49A and IB-22A), iron formation (IB-32 and IB-47A), and marble (IB-41A) exhibit an enrichment pattern in HREE over MREE, which is a pattern similar to the marine signature (Piper and Bau 2013).

6.4 Degree of oxygenation of the paleoenvironment

The ionic states of Cerium (Ce) depend on the degree of oxygenation of seawater. In anoxic environments, such as the Archean atmosphere, there was no Ce fractionation causing the Ce/Ce* ratio to be close to 1. With increasing oxygen content in the Paleoproterozoic atmosphere Ce fractionation began to occur, generating Ce/Ce* anomalies between 1-0.55 (Kamber and Webb 2001; Bolhar and Van Kranendonk 2007). Nowadays, the seawater is oxygenated and exhibits strong negative anomalies of Ce/Ce* < 0.55 (Planavsky et al. 2010).

Diagenetic effects and/or percolation of hydrothermal fluids generated a slight enrichment in LREE and MREE observed in the host and country rocks (Bau and Duslki 1996; Webb and Kamber 2000). Despite these changes, the Ce/Ce* anomalies are mostly positioned in the true negative anomaly field indicating oxic conditions for the source and host depositional environment (Figure 12A), with only one source sample exhibiting a positive Ce anomaly (IB-46).
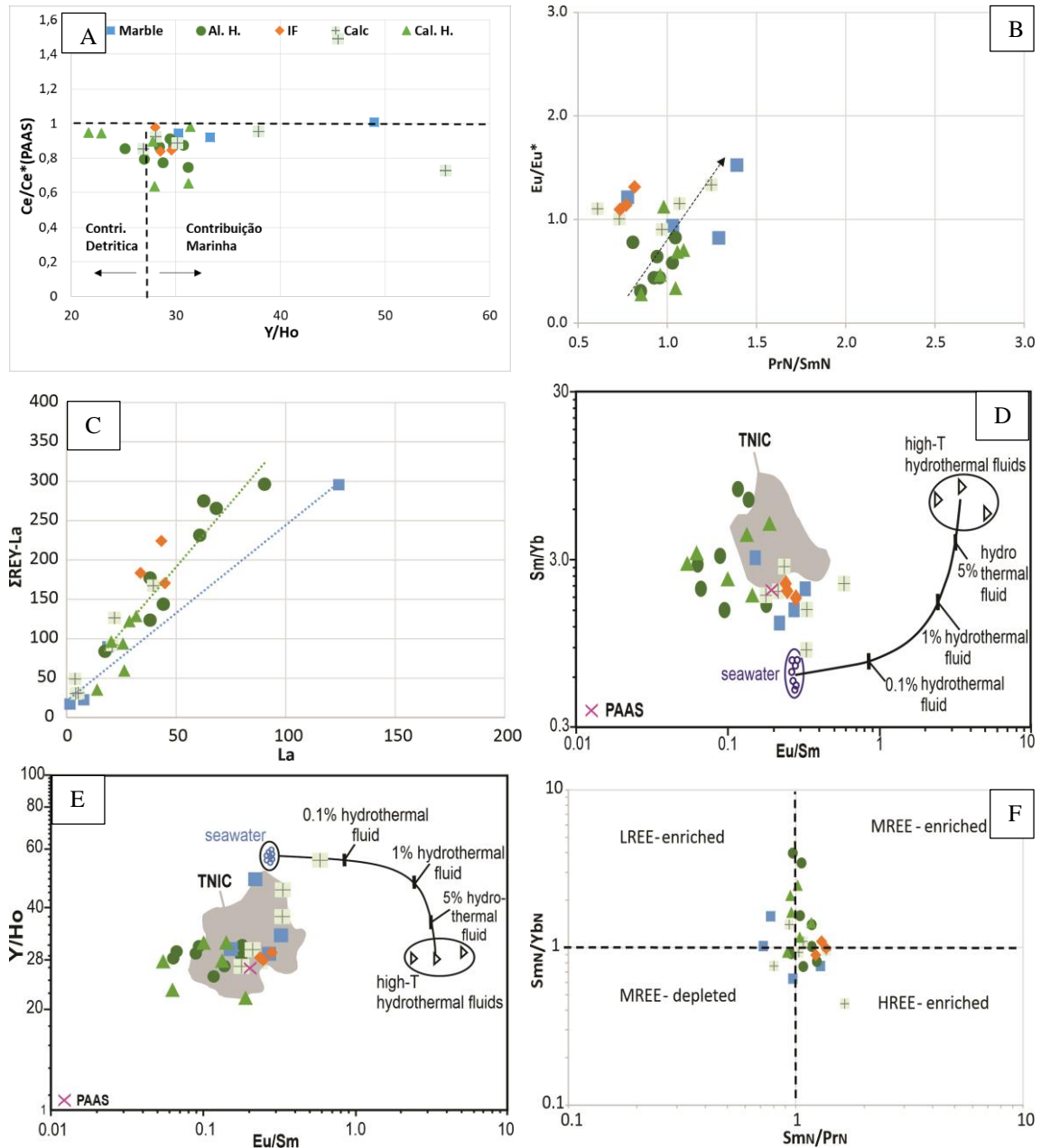
Figure 11: Diagrams for geochemical discrimination of primary signature change. A. Ratio of Y/Ho x Ce/Ce* differentiating detrital and marine contribution (Kamber and Webb 2001; Ling et al. 2013; Ribeiro et al. 2021. B. PrN/SmN x Eu/Eu* plot indicates a positive correlation between ratios suggesting that Eu was not dissociated from REY in redox reactions during diagenesis. C. Plot of La x ΣREY-La, a positive correlation is noted and some scattering of the samples which points to fluid influence (Manikyamba et al. 1993). D. Eu/Sm x Sm/Yb plot indicating signature near Fe-Mn hydrogenic crusts (Alexander et al. 2008). E. Plot of Eu/Sm x Y/Ho samples plot near the field of Fe-Mn crusts and show slight scatter which may be generated due to fluid influence (Alexander et al. 2008). CTNI samples (Ribeiro 2021). Plot of SmN/PrN x SmN/YbN enrichment classification of REE groups indicating slight enrichment of LREE and MREE of the samples (Samala et al. 2018). Sea. Marbles. H. Al - Aluminous Hosts. H. Lime. Carbonaceous Hosts. Calc. Calcissilic.

From the analysis of the negative Ce/Ce* anomalies it can be suggested that the samples exhibit oxidative conditions, similar to the calcissilicates and marbles analyzed by Ribeiro (2021) at CTNI, from 2.33 to 1.85 Ga Paleoproterozoic carbonates of the

Guanmenshan Formation, Sino-Korean Craton (Tang et al. 2013) and from Paleoproterozoic graphite mineralization in the Jingshan Group, North China Craton (Wang et al. 2019).

Uranium (U) is a sensitive element to redox reactions and it has a minor enrichment in oxic to suboxic environments where it is in the soluble form of U^{6+} or as non-reactive chemical complexes ($UO^2(CO^3)^{4-}$), occurring in oxygenated environments (e.g. modern continental margin sediments) in concentrations below 10 ppm (Algeo and Maynard 2004). Thorium (Th), in contrast, is concentrated during weathering and also in resistate minerals such as clays and heavy minerals, respectively (Jones and Manning 1994; Rimer 2004; Tobia and Mustafa 2016). In Figure 12B, it is observed that most of the samples are plotted in the U/Th ratio field <0.75 indicating an oxic paleoenvironmental condition, corroborating with the Ce/Ce* anomalies.

The low enrichment of Mo (<100 ppm) suggests that Mo is associated with the adsorption of these metal on clay minerals since, in reducing environments, there would be an enrichment in Mo correlated to precipitation of sulfides (Xu et al. 2012).
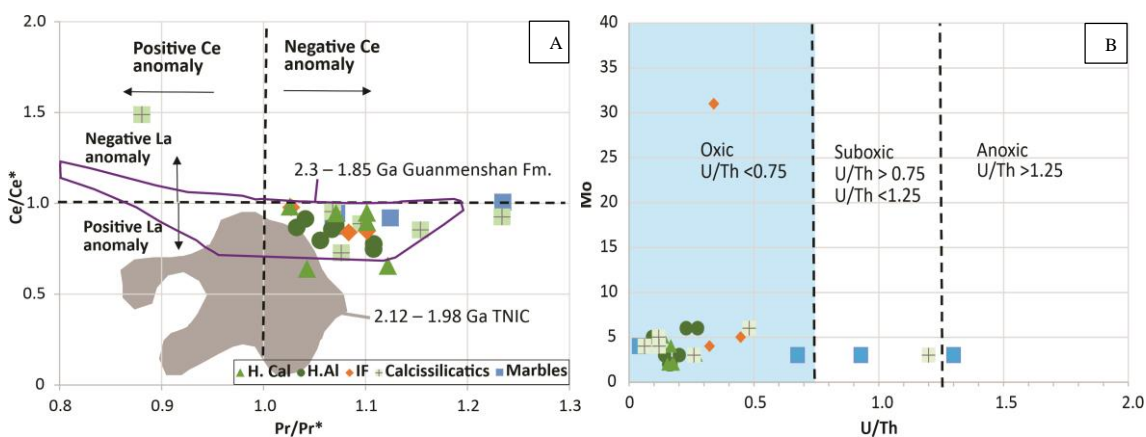

Figure12: Chemical diagrams indicating oxygen availability in geological environments. A. Pr/Pr* x Ce/Ce* plot proposed by Bau and Dulski (1996) indicating that most samples are plotted in the field of true negative Ce anomalies, suggesting an oxidizing environment; Guanmenshan Fm. (Tang et al. 2013); and CTNI (Ribeiro 2021). F. Graph adapted from Jones and Manning (1994); McKirdy et al. (2011), comparing Mo x U/Th, note the intersecting fields that corroborate the character of the oxic paleoenvironment of the samples.

6.5 Trace elements and their relationship with total graphitic carbon

In the petrographic observations, it could be defined that the syngenetic graphites formed during metamorphism and consequent graphitization of possible organic matter present in sedimentary protoliths occur mostly, while the epigenetic ones formed by fluid

percolation occur secondarily. Therefore, as the majority of syngenetic graphites occur, it will be considered that the organic carbon was transformed into graphite and analyzed as Total Graphitic Carbon (TGC) to evaluate its correlation with paleoenvironmental and paleoproductivity trace elements.

Based on the analysis of the CaO + MgO vs. TGC graph, it is observed a high positive correlation in the aluminous host rocks (R^2=0.75), phenomenon less noticeable in carbonate rocks which showed a weak positive correlation with R^2=0.49. That weak correlation in carbonate host rocks suggests that graphitic carbon already is already present in the protolith and would not be derived mainly from reactions with carbonate (Figure 13A).

Sulfur (S) is present in anoxic environments and in organic matter-rich sediments as a consequence of the sulfate-reducing bacteria. Sulfate reduction occurs when all the other oxidants such as O2> Oxides-Mn> NO3> Oxides-Fe have been used and are depleted in oxigen (Marz et al. 2009). A moderate negative correlation between TGC and S (R^2=0.55) for the aluminous host rocks is shown in Figure 9B, while there is a weak positive correlation with R^2=0.49 (Figure 9B) for the carbonate host rocks. These results indicate the existence of low interaction of sulfate-reducing bacteria due to the existence of an oxidizing paleoenvironment as shown by anomalies of Ce/Ce*, U/Th ratio, pyrites' texture in microcrystals, as well as infilled framboids pyrite that suggest the precipitation of diagenetic pyrites in an oxic-suboxic environment (Liu et al. 2019).

Titanium (Ti) is an element associated with detrital origin, whereas Phosphorus (P) and Barium (Ba) are primarily related to paleoproductivity of biogenic origin (Algeo et al. 2011). Therefore, the P/Ti ratio was used to normalize paleoproductivity in relation to the detrital input (Calvert and Pedersen 1993; Ferryday and Montenari 2016).

The results indicate that the aluminous host rocks have a strong negative correlation with the TGC with an R^2=0.80. It denotes that TGC is correlated with P and the paleoproductivity of the depositional paleoenvironment, while the carbonate host rocks exhibit a low positive correlation with an R^2 = 0.30 (Figure 9C). The low positive correlation in the carbonate host rocks between TGC and P/Ti ratio can be attributed to the precipitation of diagenetic pyrites. Pyrite's precipitation diminishes the potential of Fe-redox pumping, even close to an oxidizing environment, which makes the bacterial sulfate reduction mechanism ineffective as a phosphogenesis booster. It happens because the phosphate is released into the water column and efficiently recycled, not being fixed as francolite in the sediment (Pufhal and Hiatt 2012).

The association in the carbonate host rocks between TGC and the Ba/Ti ratio shows an $R^2=0.55$ (Figure 9D), suggesting that there is a moderate positive correlation involving TGC and the paleoproductivity attributed to Ba (Dean et al. 1997; Algeo and Maynard 2004). It is also worth mentioning that this moderate correlation of TGC with Ba may indicate the remobilization of Ba during metamorphism and/or the precipitation of barite from the oxidation of organic sulfides (Odin et al. 2016).

Nickel (Ni) is a sulfide-forming element, redox-sensitive, and an important nutrient involved in the biological cycle during primary production, but when in excess it becomes a biolimiting element (Lipinski et al. 2003; Tribovillard et al. 2006). In oxic and suboxic environments, as indicated by tracer elements in this work, Ni is soluble as a cation (Ni^{2+}, $NiCl^+$) or is adsorbed on humic or fulvic acids (Tribovillard et al. 2006). Figure 9E exhibits a moderate negative correlation with the aluminous host rocks with an $R^2=0.56$, and a strong negative correlation with the carbonate host rocks ($R^2=0.77$). The moderate correlation of Ni with TGC in the aluminous host rocks may be related to its dissociation in clay minerals because of diagenetic processes (Ferryday and Montenari 2016).

Copper (Cu), a redox-sensitive element precipitated by autonomous sulfides or coprecipitated with Fe-sulfides, it is also present in the biocycle, fixing itself in reducing conditions in sediments through organic matter and during the formation of clay minerals such as nontronite and smectite (Algeo and Maynard 2004). Figure 9F presents strong negative correlations with both the aluminous host rocks with an $R^2=0.90$, and the carbonate host rocks an $R^2=0.71$. The strong negative correlation of TGC with Cu, noticed in both groups of host rocks, might suggest Cu fixation through organic matter (Tribovillard et al. 2006), even under confined reducing conditions.

Isotope data performed in the study area by Oliveira and Sighinolfi (1983) on carbonate-bearing phosphates as well as their frequent association with extensive layers of graphite, suggest organic phosphate precipitation in which graphite and carbonates would be the consequence of an intense deposition of organic debris.

The Y/Ho ratio in the host rocks ranges from 21.65 to 31.38 with values near the PAAS, which points to a detrital contribution, whereas in the country rocks this ratio varies from 26.92 to 55.80, suggesting a higher marine contribution. Some aluminous host rocks (IB-19B and IB-79), calc-silicate rocks (IB-49A and IB-22A), iron formations (IB-32 and IB-47A), and marble (IB-41A) exhibit enrichment pattern of HREE over MREE, which is a pattern similar to the marine signature (Ribeiro 2021). Combining that

information alongside the correlations of TGC with the ratios of P/Ti, Ba/Ti, and with the Ni and Cu metals, leads to suggest that the deposition of organic matter is associated with paleoproductivity in a paleoenvironment with marine and detrital influence.

This association is suitable to the recent models of Precambrian phosphogenesis (Papineau 2009; Nelson et al. 2010), which is in congruence with the results found in the area by Ribeiro (2021). Based on these authors, the contribution of sediments rich in P and Fe-oxyhydroxide is originated from the continent after deglaciation and chemical weathering, increasing the primary productivity on the coastline and promoting francolite precipitation.

The growth in river flow that carries P can sustain the rise in productivity of organic carbon, which will be followed by an increase in alkalinity fluxes and detrital carbonate proportion (Kump and Arthur 1999). The presence of high productivity is regarded as an essential factor for the maintenance of sediments rich in organic matter (Piper and Calvert 2009). Therefore, the preservation of organic carbon originated from high productivity deposited in an oxidizing paleoenvironment may be the consequence of a deposition higher than the rate of degradation on the substrate (Pedersen and Calvert 1990).

7. CONCLUSION

The petrographic analyses indicate two generations of graphite. The first one, associated with the process of graphitization generated by metamorphism, is syngenetic, has a greater granulometry as well as idioblastic flakes. The second one, connected to the percolation of fluids and deposition of graphite, is epigenetic, has a smaller granulometry, occurs deposited in venules or as a consequence of carbonation, displays vermicular and botryoidal habits.

Syngenetic graphite can be classified as developed in 3 metamorphic facies. The flakes associated with the peak of metamorphism, at the granulite facies, occur in gneisses as well as developed crystals with tabular habits and straight edges. The flakes that are attributed to the amphibolite facies appear mainly in schists and marbles with smaller flakes, tabular habits, and ragged edges. Finally, there are also flakes associated with the greenschist facies that present small crystals with granular and tabular habits.
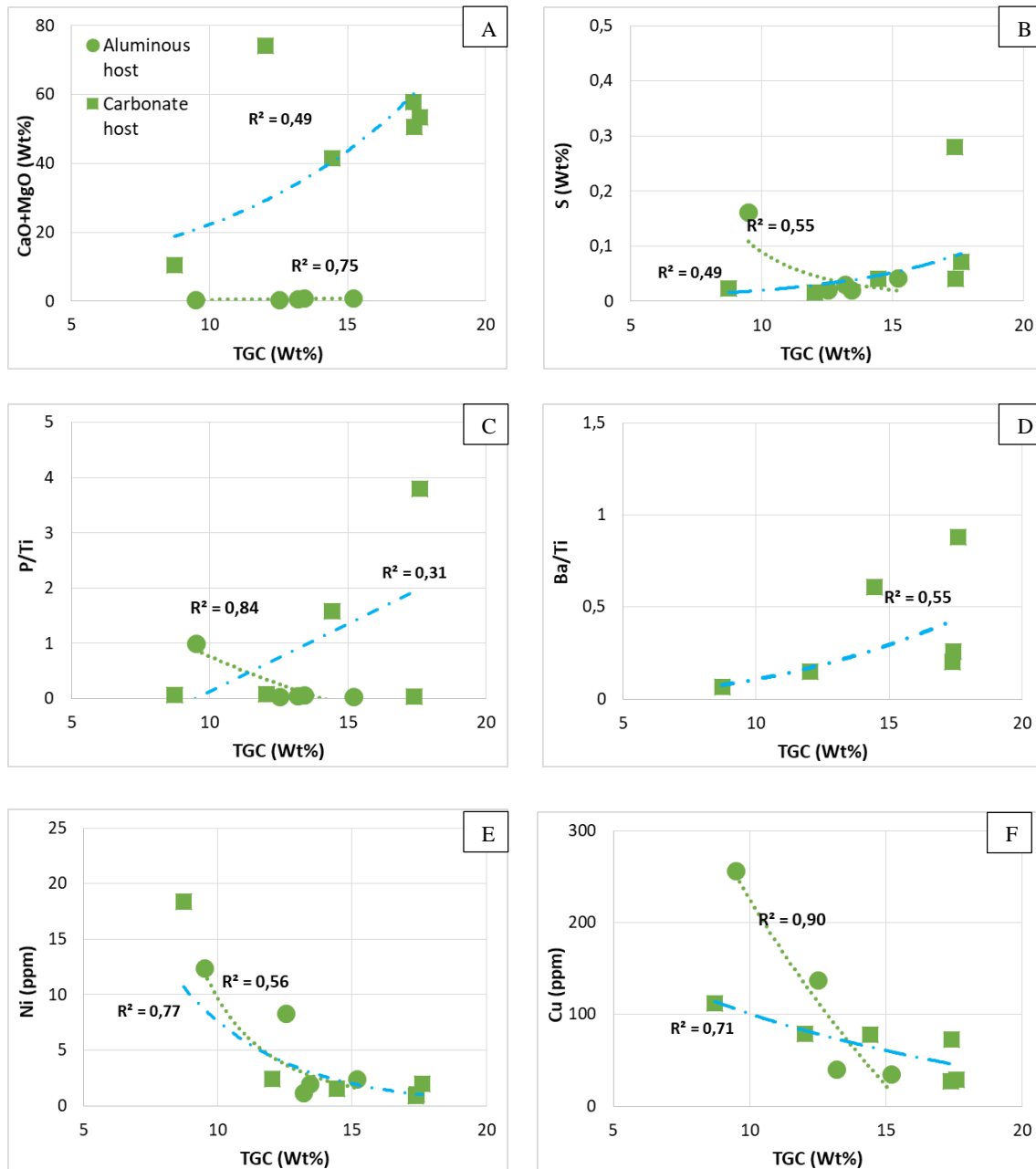
Figure 13: Geochemical diagrams showing correlations between Cg and CaO+MgO, S, P/Ti, Ba/Ti, Ni and Cu. A. Graph of Cg x CaO+MgO. B. Graph of Cg x S. C. Graph of Cg x P/Ti. D. Graph of Cg x Ba/Ti (values available only for carbonate hosts). E. Graph of Ni x Cg. F. Graph of Cu x Cg. Total graphitic carbon (TGC).

The lithogeochemical characteristics of the host and country rocks of the graphite mineralization suggest that the deposition of sedimentary protoliths is linked to a marine paleoenvironment, predominantly oxic, and influenced by detrital input. Analyzes of TGC with tracer elements indicate that correlations are still preserved, suggesting the deposition of organic matter in a context of high paleoproductivity in the paleobasin. However, isotopic data are indispensable to verify this hypothesis. The growth in paleoproductivity might have generated a conducive environment to the increase of the

detrital carbon ratios, resulting in the carbonaceous layers and the enrichment in P observed in the TNIC marbles and calc-silicate rocks.

The relation between the paleoproterozoic graphite host rocks deposited in the oxic paleoenvironment and the phosphorus anomalies of the TNIC country rocks suggest that the deposition of organic matter that originating graphite be correlated with the increase in organic paleoproductivity generated after the GOE event – Great Oxygenation Event which culminated in the first major phosphogenesis event in the geological record.

8. ACKNOWLEDGMENTS

9. REFERENCES

Alexander, B.W., Bau, M., Anderson, P., Dulski, P. 2008. Continentally-derived solutes in shallow Archean seawater: rare earth element and Nd isotope evidence in iron formation from the 2.9 Ga Pongola Supergroup, South Africa. Geochimica et Cosmochimica Acta, 72: 378-394. H.ttps://doi.org/10.1016/j.gca.2007.10.028.

Alkmim, F. F.; Neves, B. B.; Alves, J. A. C. 1993. Arcabouço tectônico do Cráton do São Francisco: uma revisão. O Cráton do São Francisco, 45-62.
Almeida, F. F. M. 1977. O Cráton do São Francisco. Revista Brasileira de Geociências v. 7, p 349-364.

Algeo, T.J., and Maynard, J.B. 2004. Trace-element behavior and redox facies in core shales of Upper Pennsylvanian Kansas-type cyclothems. Chem. Geol. 206 (3 e 4), 289 e 318.

Algeo T J, Kuwahara K, Sano H. 2011. Spatial variation in sediment fluxes, redox conditions, and productivity in the Permian-Triassic Panthalassic Ocean. Palaeogeogr Palaeoclimatol Palaeoecol, 308: 65–83.

Aoya M., Kouketsu Y., Endo S. 2010. Extending the applicability of the Raman carbonaceousmaterial geothermometer using data from contact metamorphic rocks. Journal of Metamorphic Geology 28, 895–914.

Barbosa, J. S., Sabaté, P. 2004. Archean and Paleoproterozoic crust of the São Francisco cráton, Bahia, Brazil: geodynamic feactures. Precambrian Research, 133(3): 1-27.

Bau, M. 1993. Effects of syn-depositional and postdepositional processes on the rare-earth elemento distribution in Precambrian iron-formations. European Journal of Mineralogy, 5: 257- 267.

Bau, M. and Dulski, P, 1996. Distribution of yttrium and rare-earth elements in the Penge and Kuruman iron-formations, Transvaal Supergroup, South Africa. Precambrian Research, 79 (2): 37-55. https://doi.org/10.1016/0301-9268(95)00087-9.

Bau, M., Möller, P., Dulski, P., 1997. Yttrium and lanthanides in eastern Mediterranean seawater and their fractionation during redox-cycling. Marine Chemistry, 56: 123–131. https://doi.org/10.1016/S0304-4203(96)00091-6.

Bau, M. 1999. Scavenging of dissolved yttrium and rare earths by precipitating iron oxyhydroxide: experimental evidence for Ce oxidation, Y-Ho fractionation, and lanthanide tetrad effect. Geochim. Cosmochemistry, Acta, 63: 67–77. https://doi.org/10.1016/S0016-7037(99)00014-9.

Bhattacharya S, Choudhary AK, Basei, M. 2012. Original nature and source of khondalites in the Eastern Ghats province, India. In: Mazumder R, Saha D (eds) Palaeoproterozoic of India. Geol Soc Lond Spec Publ 365:145–158.

Belém, J. 2006. Caracterização mineralógica, física e termobarométrica de minérios de grafita da Província Grafítica Bahia-Minas. Dissertação de Mestrado, Instituto de Geociências, Universidade Federal de Minas Gerais, 165 p.

Bolhar, R., Kamber, B. S., Moorbath, S., Fedo, C. M., Whitehouse, M. J. 2004. Characterisation of early Archaean chemical sediments by trace element signatures. Earth and Planetary Science Letters 222, 43–60.

Bolhar, R. and Van Kranendonk, M.J. 2007. A non - marine depositional setting for the northern Fortescue Group, Pilbara Craton, inferred from trace element geochemistry of stromatolitic carbonates. Precambrian Research, 155: 229 - 250. https:// doi.org/ 10.1016/ j.precamres. 2007.02.002.

Bucher, K. and Grapes, R. 2010. 8th ed. Petrogenesis of metamorphic rocks, 144p.
Buseck P.R., Beyssac, O. 2014. Graphitic carbon: from organic matter to graphite: graphitization. Elements. 10:421–426.

Calvert, S.E., Pedersen, T.F., 1993. Geochemistry of Recent oxic and anoxic marine sediments: implications for the geological record. Mar. Geol. 113 (1 e 2), 67 e 88.

Courtois, C. and Treuil, M. 1977. Distribution des terres rares et de quelques éléments en trace dans les sédiments récents des fosses de la Mer Rouge. Chem. Geol. 20: 57–72.

Dean W E, Gardner J V, Piper D Z. Inorganic geochemical indicators of glacial-interglacial changes in productivity and anoxia on the California continental margin. Geochim Cosmochim Acta, 1997, 61: 4507–4518.

Dash, B., Sahoo, K. N. and Bowes, D. R. 1987. Geochemistry and original nature of Precambrian khondalites in the Eastern Ghats, Orissa, India. Transactions of the Royal Society of Edinburgh, Earth Science, 78, 115–127.

Ferryday, T. and Montenari, M. 2016. Chapter Three - Chemostratigraphy and Chemofacies of Source Rock Analogues: A High-Resolution Analysis of Black Shale Successions from the Lower Silurian Formigoso Formation (Cantabrian Mountains, NW Spain), Editor(s): Montenari, M., Stratigraphy & Timescales, Academic Press, Vol 1, 123-255 p. https://doi.org/10.1016/bs.sats.2016.10.004.

Fleischer, M. Parker, R. L. 1967. Composition of the earth's crust, by Raymond L. Parker In: Fleischer, M. Parker, R. L (eds). Data of Geochemistry: Composition of The Earth's Crust, Chapter D. Geological Survey, 6 ed. 23p.

Floyd, P., Winchester, J., Park, R., 1989. Geochemistry and tectonic setting of Lewisian clastic metasediments from the early Proterozoic Loch Maree Group of Gairloch, NW Scotland. Precambrian. Res. 45 (1), 203 and 214.

French, B.M., and Rosenberg, P.E., 1965. Siderite (FeCO3): termal decomposition in equilibrium with graphite. Science 147, 1283– 1284.

Galvez, M. E., Beyssac, O. Martinez, I. Benzerara, K. Chaduteau, C., Malvoisin, B. Malavieille, J. 2013. Graphite formation by carbonate reduction during subduction. Nature Geoscience. DOI: 10.1038/NGEO1827.

GeoSGB, 2021. Arquivos vetoriais das ocorrências minerais do estado da Bahia. Disponível em: https://geosgb.cprm.gov.br/.

Herron, M.M., 1988. Geochemical classification of terrigenous sands and shales from core or log data. J. Sediment. Res. 58 (5), 820 - 829.

Jara, A. D., Betemariam, A., Woldetinsae, G., Kim, J. Y. 2019. Purification, application and current market trend of natural graphite: A review. International Journal of Mining Science and Technology. Vol. 29, p. 671–689.

Ji, H., Shimazaki, H., Hu, S., Zhao, Y. 1994. Occurrence and geochemistry of khondalite series in the Shandong Peninsula, China. Resource Geology, 44(1), p. 39-49.

Jones B., and Manning, D.A.C. 1994. Comparison of geochemical indices used for the interpretation of palaeoredox conditions in ancient mudstones. Chemical Geology, v. 111, p. 111-129.

Kamber, B.S., Webb, G.E., 2001. The geochemistry of late Archean microbial carbonate: implications for ocean chemistry and continental erosion history. Geochimica et Cosmochimica Acta, 65 (15): 2509-2525.

Khan, R. M. K., Das Sharma S., Patil, D. J., Naqvi S. M. 1996. Trace, rare-earth element, and oxygen isotopic systematics for the genesis of banded iron-formations: evidence from the Kushtagi schist belt, Archaean Dharwar Craton, India. Geochim. Cosmochim. Acta 60, 3285–3294.

Khelen, A.C., Manikyamba, C., Subramanyamb, K.S.V., Santosh, M., Gangulye, S., Kalpanab, M.S., Subba Raob, D.V. 2019. Archean seawater composition and depositional environment – Geochemical and isotopic signatures from the stromatolitic carbonates of Dharwar Craton, India. Precambrian Research, v. 330, p. 35–57.

Klein, C. and Dutrow, B. 2012. Manual de Ciência dos Minerais, 23a ed. Bookman.

Klein, C. and Beukes, N. J. 1989. Geochemistry and sedimentology of a facies transition from limestone to iron-formation deposition in the Early Proterozoic Transvaal Supergroup, South Africa. Econ. Geol. 84, 1733–1774.

Keeling, J., 2017, Graphite: Properties, uses and south Australian resources: MESA Journal, v. 84, p. 28–41.

Kump, L., and Arthur, M. A. 1999. Interpreting carbon-isotope excursions : Carbonates and organic matter. Chemical Geology, 161(1), 181-198. https://doi.org/10.1016/S0009-2541(99)00086-8.

Kosin, M. D., Melo, R.C., Souza, J.D., Oliveira, E.P., Carvalho, M.J.; Leite, C.M.M. 2003. Geologia do segmento norte do Orógeno Itabuna-Salvador-Curaçá e guia de excursão. Revista Brasileira de Geociências, São Paulo, 33(1): 15-26.

Kwiecińska, B., and Petersen, H.I., 2004. Graphite, semi-graphite, natural coke, and natural char classification—ICCP system. International Journal of Coal Geology, 57, 99-116.

Ling, H., Xi, C., Li, D., Wang, D., Shields-Zhou, G., Zhu, M, 2013. Cerium anomaly variations in Ediacaran – earliest Cambrian carbonates from the Yangtze Gorges área, South China : Implications for oxygenation of coeval shallow seawater. Precambrian Research, 225: 110-127. https://doi.org/ 10.1016/ j.precamres.2011.10.011.

Liu, Z., Chen, D., Zhang, J., Lu, X., Wang, Z., Liao, W., Shi, X., Tang, J., Xie, G. 2019. Pyrite Morphology as an Indicator of Paleoredox Conditions and Shale Gas Content of the Longmaxi and Wufeng Shales in the Middle Yangtze Area, South China. Minerals, 9, 428; doi:10.3390/min9070428.

Lipinski, M., Warning, B., Brumsack, H., 2003. Trace metal signatures of Jurassic/Cretaceous black shales from the Norwegian shelf and the Barents sea. Palaeogeogr. Palaeoclimatol. Palaeoecol. 190 (0), 459 e 475.

Luque, F.J., Rodas, M., Galán, E., 1992. Graphite vein mineralization in the ultramafic rocks of southern Spain: mineralogy and genetic relationships. Mineralium Deposita 27, 226–233.

Luque, F.J., Barrenechea, J. F., Rodas, M. 1993. Graphite geothermometry in low and high temperature regimes: two case studies: Geological Magazine, v. 130, p. 501-51.

Marz, C., Beckmann, B., Franke, C., Vogt, C., Wagner, T., Kasten, S., 2009. Geochemical environment of the ConiacianeSantonian western tropical Atlantic at Demerara rise. Palaeogeogr. Palaeoclimatol. Palaeoecol. 273 (3 e 4), 286 e 301.

Mclennan, S. M.1989. Rare earth elements in sedimentary rocks ; influence of provenance and sedimentary processes. Reviews in Mineralogy and Geochemistry, 21(1): 169-200.
Manikyamba, C., Balaram, V., Naqvi, S.M. 1993. Geochemical signatures of polygenetic origin of a banded iron formation (BIF) of the Archaean Sandur greenstone belt (schist belt) Karnataka nucleus, India. Precambrian Research, v. 61, p. 137-164.

Manoel, T.N. and Leite, J.A.D. 2018. On the origin of the Neoproterozoic Peresopolis graphite deposit, Paraguay Belt, Brazil. Journal of South American Earth Sciences, 84, 104-112.

Martín-Méndez, I., Boixereu, E., Villaseca, C. 2016. Mineralogical and isotopic characterization of graphite deposits from the Anatectic Complex of Toledo, central Spain. Miner Deposita. 51:575–590. DOI 10.1007/ s00126- 015-0625-9.

McKirdy, D. M., Hall, P.A., Nedin, C., Halverson, G.P., Michaelsen, B.H., Jago, J.B., Gehling, J.G., Jenkins, R.J.F. 2011. Paleoredox status and thermal alteration of the lower Cambrian (Series 2) Emu Bay Shale Lagerstätte, South Australia, Australian Journal of Earth Sciences: An International Geoscience Journal of the Geological Society of Australia, 58:3, 259-272.

Nakamura, Y. and Akai, J. 2013. Microstructural evolution of carbonaceous material during graphitization in the Gyoja-yama contact aureole: HRTEM, XRD and Raman spectroscopic study. Journal of Mineralogical and Petrological Sciences, v. 108, p. 131-143.

Nelson, G. J.; Pufhal, P. K.; Hiatt, E. E. 2010. Paleoceanographic constraints on Precambrian phosphorite accumulation, Baraga Group, Michigan, USA. Sedimentary Geology, 226 (1-4): 9-21. https:// doi.org/ 10.1016/ j.sedgeo. 2010.02.001.

Nozaki, Y.; Zhang, J.; Amakawa, H. 1997. The fractionation between Y and Ho in the marine environment. Earth and Planetary Science Letters, 148: 329-340. https://doi.org/10.1016/S0012-821X(97)00034-4.

Odin, G.P., Oulfa, B., Cabaret, T., Foy, E. Rouchon, V. 2016. Alterations of fossil-bearing shale (Autun, France; Permian), part III: Framboidal pyrite and sulfur as the main cause of efflorescence. Annales de Paléontologie, http:// dx.doi.org /10.1016 /j.annpal. 2016.01.001.

Oliveira, E.P., Carvalho, M.J., McNaughton, N.J. 2004. Evolução do segmento norte do Orógeno Itabuna-Salvador-Curaçá: Cronologia da acresção de arcos, colisão continental e escape de terrenos. Boletim Geologia USP, Série Científica, v. 4, 41-53 p.

Oliveira, E.P., McNaughton, N.J., Armstrong, R. 2010. Mesoarchaean to Paleoproterozoic growth of the northern segment of the Itabuna–Salvador–Curaçá orogen, São Francisco craton, Brazil. Geological Society, London, Special Publications, v. 338, 263-286 p.

Oliveira, M. A. F. T and Sighinolfi, G. P. 1983. Geochemstry of Precambrian phosphate –carbonate intrusives from Bahia (Brazil). Geochemical Journal, vol. 17, pp. 277-287.
Pasteris, J. D. and Wopenka, B. 1991. Raman spectra of graphite as indicators of degree of metamorphism. Canadian Mineralogist, 29, 1–9.

Papineau, D. 2010. Global biogeochemical changes at both ends of Proterozoic: insights from phosphorites. Astrobiology, 10 (2): 165-181.

Papineu, D., Purohit R., Fogel M., Shields-zhou, G.A. 2013. High phosphate availability as a possible cause for massive cyanobacterial production of oxygen in the Paleoproterozoic atmosphere. Earth and Planetary Science Letters, 362: 225-236.

Pedersen, T.F., Calvert, S.E., 1990. Anoxia vs productivity; what controls the formation of organic-carbon-rich sediments and sedimentary rocks? AAPG Bull. 74 (4), 454 e 466.

Pedrosa-Soares A.C., Faria L.F., Reis L.B. 1999. The Minas-Bahia Graphite Province, eastern Brazil: mineralization controls and types. In: European Union Geosciences, Strasbourg. Abstract H04: 4A/09: F5, p. 493.

Pereira, R. M., Neumann, R., Salomão, M., Guimarães, P.V., Ramos, G.V., Dutra, A.C., Pedroso, E. 2016. Terrenos khondalíticos: principais domínios para manganês, grafita, ouro e zinco no estado do Rio de Janeiro e regiões limítrofes. Geonomos, 24(1), 41-51.

Piaia, P., Oliveira, E.P., Valeriano, C.M. 2017. The 2.58 Ga São Jose do Jacuípe gabbro-anorthosite stratiform complex, Itabuna-Salvador-Curaçá Orogen, São Francisco Craton, Brazil: Root of the Neoarchaean Caraíba continental arc? Journal of South American Earth Sciences, v. 79, 326 – 341 p.

Piper, D.Z., Calvert, S.E., 2009. A marine biogeochemical perspective on black shale deposition. Earth-Science Rev. 95 (1 e 2), 63 e 96.

Piper, D.Z, Bau, M. 2013. Normalized Rare Earth Elements in Water, Sediments, and Wine: Identifying Sources and Environmental Redox Conditions. American Journal of Analytical Chemistry, 4: 69-83. http:// dx.doi.org/ 10.4236/ ajac.2013.410A1009.

Planavsky, N., Bekker, A., Rouxel, O. J., Kamber, B., Hofmann, A., Kkudsen, A., Lyons, T. W. 2010. Rare earth element and yttrium compositions of Archean and Paleoproterozoic Fe formations revisited: new perspectives on the significance and mechanisms of deposition. Geochimica et Cosmochimica, 74: 6387-6405. https://doi.org/10.1016/j.gca.2010.07.021.

Pufahl, P.K. 2010. Bioelemental sediments, In: James, N.P., and Dalrymple, R.W., eds., Facies models, 4th ed.: Geological Association of Canada, p. 477–503.

Pufahl, P. K.; Hiatt, E. E. 2012. Oxygenation of the Earth's atmosphere-ocean system: a review of physical and chemical sedimentologic responses. Marine and Petroleum Geology, 32(1): 1-20. https://doi.org/10.1016/j.marpetgeo.2011.12.002.

Ramsay, J. G. and Huber, M. I. 1987. The Techniques of Modern Structural Geology. Volume 2: Folds and Fractures. Academic Press, London, 391 pp. DOI: https://doi.org/ 10.1017/ S0016756800010384.

Reynard, B., Lecuyer, C., Grandjean, P. 1999. Crystal-chemical controls on rare-earth elemento concentrations in fossil biogenic apatites and implications for paleoenvironmental reconstructions. Chemical Geology, 155: 233–241.

Ribeiro, T.S., Misi, A., Oliveira, L.R.S., Sá, J.H.S., Debruyne, D., Câmara, I.S. Evidence of Paleoproterozoic phosphogenesis in the Salvador-Curaçá Orogen (Tanque Novo-Ipirá Complex), northeastern São Francisco Craton, Brazil. Braz. J. Geol. 51 (03); 2021. https://doi.org/10.1590/2317-4889202120190137.

Rimmer, S.M. 2004. Geochemical paleoredox indicators in Devoniane Mississippian black shales, Central Appalachian Basin (USA). Chem. Geol. 206 (3 e 4), 373 e 391.

Samala, W., Khirekesh, Z., Amini, A., Bafti, B.S. 2018. Diagenetic evolution of the upper Devonian phosphorites, Alborz Mountain Range, northern Iran. Sedimentary Geology. 376, 90–112.

Scherba, C., Montreuil, J.F., Barrie, C. T. 2018. Geology and Economics of the Giant Molo Graphite Deposit, Southern Madagascar. Society of Economic Geologists, Inc. SEG Special Publications, no. 21, pp. 347–363.

Schlumberger, 2009. Log Interpretation Charts, 2009 Ed. Schlumberger, Texas.

Scogings, A. 2019. Graphite Mineral Notes - geology, petrography, production, markets, specifications. Published on LinkedIn.

Shields, G. and Stille, P. 2001. Diagenetic constraints on the use of cerium anomalies as palaeoseawater redox proxies: an isotopic and REE study of Cambrian phosphorites. Chemical Geology, 175: 29–48. https://doi.org/ 10.1016/ S0009-2541(00)00362-4.

Silva, L.C.; Mcnaughton, N.J.; Melo, R.C.; Fletcher, I.R. U-Pb SHRIMP ages in the Itabuna- Caraíba TTG high-grade complex: the first window beyond the Paleoproterozoic overprinting of the eastern Jequié craton, NE Brazil. In: International symposium on granites and associated mineralizations, 2., 1997. Salvador. Proceedings. Salvador: Sociedade Brasileira de Geologia, 1997. p. 282-283.

Silva, M. G., Misi, A. 1998. Embasamento Arqueano-Proterozóico Inferior do Cráton do Sào Francisco, no Nordeste da Bahia: geologia e depósitos minerais. Salvador, SGM, 164 p. (Série Roteiros Geológicos).

Simonen, A. 1953. Stratigraphy and sedimentation of the svecofenidic, early Archean supracrustal rock in south-western Finland. Bulletin Commission Geological Finland, 160, 64.

Tang, H.S., Chen, Y.J., Santosh, M., Zhong, H., Yang, T., 2013. REE geochemistry of carbonates from the Guanmenshan Formation, Liaohe Group, NE Sino-Korean Craton: implications for seawater compositional change during the Great Oxidation Event. Precambrian Research.

Teixeira, L. R. 1997. O Complexo Caraíba e a Suíte São José do Jacuípe no Cinturão Salvador-Curaçá (Bahia, Brasil): petrologia, geoquímica e potencial metalogenético. Tese de Doutorado – Instituto de Geociências, Universidade Federal da Bahia, Salvador, 208 p.

Teixeira, W., Oliveira E. P., Peng, P., Dantas, E. L., Hollanda, M. H. B. M. 2017. U-Pb geochronology of the 2.0 Ga Itapecerica graphite-rich supracrustal succession in the São Francisco Craton: Tectonic matches with the North China Craton and paleogeographic inferences. Precambrian Research vol. 293 p. 91–111.

Tobias, F. and Mustafa, B.H. 2016. Geochemistry and mineralogy of the Al-rich shale from Baluti formation, Iraqi Kurdistan region: implications for weathering and provenance. Arab J. Geosci. 9:757.

Tostevin, R., Shields, G.A., Tarbuck G.M., HE.T., Clarkson, M.O., Wood, R.A. 2016. Effective use of cerium anomalies as a redox proxy incarbonate-dominated marine settings. Chemical Geology, 438: 146 – 162.

Tribovillard, N., Algeo, T.J., Lyons, T., Riboulleau, A., 2006. Trace metals as paleoredox and paleoproductivity proxies: an update. Chem. Geol. 232 (1 e 2), 12 e 32.

Wada H, Tomita T, Matsuura K, Iuchi K, Ito M, Morikiyo T. 1994. Graphitization of carbonaceous matter during metamorphism with references to carbonate and pelitic rocks of contact and regional metamorphisms, Japan. Contrib Mineral Petrol; 118:217–28.

Wang, J., Liu, J., Zhang, H., Zhang, H., Li, Y. 2019. Metamorphism, geochemistry, and carbon source on sedimentary-metamorphic graphite deposits in eastern Shandong, China. Geological Journal. p. 1–22. DOI: 10.1002/gj.3621.

Walker, T. L. 1902. The geology of Kalahandi State, Central Provinces, India. U.S. Geol. Surv. Memoirs, 33, part 3.

Webb G. E., and Kamber B. S. 2000. Rare earth elements in Holocene reefal microbialites: A new shallow seawater proxy. Geochim. Cosmochim, 64: 1557–1565. https://doi.org/10.1016/S0016-7037(99)00400-7.

Whitney, D. and Evans, B.W. 2010. Abbreviations for names of rock-forming minerals. American Mineralogist, Volume 95, pages 185–187. DOI: 10.2138/am.2010.3371.
Winter, J.D. 2009. Principles of igneous and metamorphic petrology. Prentice-Hall, New York, NY.

Xu, L.G., Lehmann, B., Mao, J.W., Nägler, T.F., Neubert, N., Böttcher, M.E., Escher, P., 2012. Mo isotope and trace element patterns of Lower Cambrian black shales in South China: multi-proxy constraints on the paleoenvironment. Chem. Geol., http://dx.doi.org/10.1016/j.chemgeo.2012.05.016.

Zhong, Y., Ma, X.D., Li, H.K., Zhaid M.G. 2019. Revisit and comparative analysis of the typical graphite deposits in the Paleoproterozoic khondalite series, western North China Craton: Implications for genesis, depositional environment and prospecting potential. Ore Geology Reviews, v. 109, p. 370–380.

CAPÍTULO 3 – CONCLUSÕES

As análises petrográficas identificaram duas gerações de grafita, uma associada a processo de grafitização gerado pelo metamorfismo – singenética que apresenta uma maior granulometria e flakes idioblásticos. A segunda geração de grafita é atribuída à percolação de fluidos hidrotermais com deposição de grafita – epigenética, marcada por uma menor granulometria, depositada em vênulas ou resulta de reações de carbonatação; têm hábitos vermiculares e botroidais.

A grafita singenética pode ser classificada como desenvolvida em 3 fácies metamórfica, onde os flakes associados ao fácies granulito, pico do metamorfismo, ocorrem em gnaisses grafitosos como cristais bem desenvolvidas com hábitos tabulares e bordas retas. Os flakes atribuídos ao fácies anfibolito são menores, tabulares e com bordas esfarrapadas registrados principalmente nos xistos e mármores grafitosos. Nessas rochas também ocorrem microcristais associados ao fácies xisto verde que se apresentam em hábitos granulares a pequenos cristais tabulares.

As características litogeoquímicas das rochas hospedeiras e encaixantes da mineralização de grafita sugerem que a deposição dos protólitos sedimentares estejam associados a um paleoambiente marinho, predominantemente óxico e com influência de aporte detrítico. As análises do Cg com os elementos traçadores indicam que as correlações ainda estão preservadas sugerindo a deposição da matéria orgânica em um momento de alta paleoprodutividade, entretanto dados isotópicos são indispensáveis para a averiguação dessa hipótese. O aumento da paleoprodutividade orgânica pode ter gerado ambiente propício para o aumento das razões de carbono detrítico, tendo como resultados as camadas carbonosas e o enriquecimento em P encontrado nas calcissilicáticas e mármores do CTNI.

A relação entre as rochas hospedeiras carbonosas paleoproterozoicas depositadas em paleoambiente óxido e anomalias de fósforo das encaixantes do CTNI, sugerem que a deposição da matéria orgânica que deu origem a grafita possa estar correlacionada com o aumento da paleoprodutividade orgânica gerada após o evento GOE - Grande Evento de Oxigenação que culminou no primeiro grande evento de fosfôgenese do registro geológico.

O trabalho desenvolvido nessa dissertação foi uma primeira contribuição para a caracterização das grafitas que ocorrem no Complexo Tanque Novo – Ipirá, Salvador

Curaçá, Craton do São Francsico. A caracterização e entendimento dos processos metalogenéticos formadores de depósitos minerais auxilia no desenvolvimento da pesquisa mineral o que pode trazer impactos positivos para a atividade mineral do estado da Bahia.

APÊNDICE A – JUSTIFICATIVA DA PARTICIPAÇÃO DOS CO-AUTORES

Co-autor prof. Dr. Aroldo Misi: Orientador, auxiliou na estruturação, interpretação e revisão do artigo.

Co-autor Luis Rodrigues dos Santos de Oliveira: Auxíliou na interpretação dos dados sobretudo na litogeoquímica e revisão do artigo.

Co-autor Tatiana Silva Ribeiro: Auxíliou na interpretação sobre a paleoambiência das rochas encaixantes e revisão do artigo.

Co-autor prof. Dr. José Haroldo da Silva Sá: Auxiliou na aquisição dos dados, estruturação e revisão do artigo.

Co-autor prof. Dr. Herbert Conceição: Auxiliou na aquisição dos dados e revisão do artigo.

Co-autor Pedro Ribeiro Rabelo de Santana: Auxiliou na elaboração da parte gráfica, discussão da geologia e revisão do artigo.

ANEXO A – REGRAS DE FORMATAÇÃO DA REVISTA

INSTRUCTIONS TO AUTHORS
Scope and Policy

AIMS AND SCOPE
The Brazilian Journal of Geology (BJG) is a quarterly journal published by the Brazilian Geological Society with an electronic open access version that provides an in-ternacional medium for the publication of original scientific work of broad interest concerned with all aspects of the earth sciences in Brazil, South America, and Antarctica, in-cluding oceanic regions adjacent to these regions. The BJG publishes papers with a regional appeal and more than local significance in the fields of mineralogy, petrology, geochemistry, paleontology, sedimentology, stratigraphy, structural geology, tectonics, neotectonics, geophysics applied to geology, volcanology, metallogeny and mineral deposits, marine geology, glaciology, paleoclimatology, geochronology, biostratigraphy, engineering geology, hydrogeology, geological hazards and remote sensing, providing a niche for interdisciplinary work on regional geology and Earth history.

The BJG publishes articles (including review articles), rapid communications, articles with accelerated review processes, editorials, and discussions (brief, objective and concise comments on recent papers published in BJG with replies by authors).

Manuscripts must be written in English. Companion papers will not be accepted.

ETHICS IN PUBLISHING
The BJG follows the Code of Good Scientific Practice published by the São Paulo State Research Foundation – FAPESP, see http://www.fapesp.br/boaspraticas/FAPESP-Code_of_Good_Scientific_Practice_2014.pdf.

FUNDING SOURCES
Authors should identify the sources of financial support for the research and/or preparation of the article and briefly describe the role of sponsor(s), if any, in study design; in the collection, analysis and interpretation of data; in the writing of the report; and in the decision to submit the article for publication.

COPYRIGHT AND OPEN ACCESS
Upon acceptance of an article, authors will be asked to

complete a "BJG publishing agreement" transferring the copyright to the Brazilian Geological Society.

The BJG is an open access journal which means that all articles will be freely available to the wider public and that reuse will be permitted.

CONFLICTS OF INTERESTS
All authors are requested to disclose any actual or potential conflict of interest including any financial, personal or other relationships with other people or organizations that could inappropriately influence, or be perceived to influence, their work.

SUBMISSION DECLARATION AND VERIFICATION
Submission of an article implies that the work described has not been published previously (except in the form of an abstract or as part of a published lecture or academic thesis), that it is not under consideration for publication elsewhere, that its publication is approved by all authors as well as tacitly or explicitly by the responsible authorities where the work was carried out, and that, if accepted, it will not be published elsewhere in the same form, in English or in any other language, including electronically, without the written consent of the copyright-holder. Authors should verify the originality of the article by checking for plagiarism with any available software.
In addition, the corresponding author must state that:

 The article has not been partitioned and that its con- tents are fully and independently understandable;

 The article, edited in Microsoft Word, A4 format, does not exceed 12,000 words;

 Each illustration or table is being sent in a separate file (.tif for figures);

 No text or illustration file exceeds 10 Mb;

 The authors are aware that submissions that do not comply with the "Instructions to authors" for BJG will be returned to the corresponding author;

 The authors are aware that if reviewers indicate the need for major or minor revision, they will have 30 days to make the corrections suggested by the editors;

 The authors are aware that they should carefully check and correct print proofs and return them to publishers within 48 hours to ensure the publication of the article without errors;

 The authors are aware that, should the article be accepted for publication, copyright will be transferred to the Brazilian Geological Society by sending a letter signed by all authors ("BJG publishing agreement").

SUBMISSION
Our online submission system (ScholarOne – SciELO) will guide you stepwise through the process of entering details on your article and uploading your files. The system will convert your article files to a single PDF file for use in the peer-review process. Editable fi- les (e.g., Word, LaTeX) are

required to typeset your article for final publication. All correspondence, including notification of the Editor's decision and requests for re- vision, will be sent by e-mail.

EVALUATION

Peer review: Articles will be submitted to critical analysis by least two reviewers.

Type of evaluation: Authors will be identified in the manuscripts received by the Reviewers.

Form and preparation of manuscripts

Use of word processing software

Regardless of the file format of the original submission, at revision you must provide us with an editable file of the entire article. Keep the layout of the text as simple as possible. Most formatting codes will be removed and replaced on processing the article. The electronic text should be prepared in a way very similar to that of conventional manuscripts.

To avoid errors you are strongly advised to use the 'spell-check' and 'grammar-check' functions of your word processor.

Article structure

There are no strict formatting requirements, but all manuscripts must contain the essential elements needed to convey your manuscript, for example, Abstract, Keywords, Introduction, Materials and Methods, Results, Conclusions, References, Artwork and Tables with Captions.

Divide the article into clearly defined and numbered sections. Subsections should be numbered 1.1 (then 1.1.1, 1.1.2, ...), 1.2, etc. (the abstract is not included in section numbering). Use this numbering also for internal cross-referencing: do not just refer to 'the text'. Any subsection may be given a brief heading. Each heading should appear on its own separate line.

Introduction

State the objectives of the work and provide an adequate background, avoiding a detailed literature survey or a summary of the results.

Material and methods

Provide sufficient detail to allow the work to be re-produced. Methods already published should be indicated by a reference. Only relevant modifications should be described.

Theory/calculation

A Theory section should extend, not repeat, the back-ground to the article already dealt with in the Introduction and lay the foundation for further work. In contrast, a Calculation section represents a practical development from a theoretical basis.

Results
Results should be clear and concise.

Discussion
This should explore the significance of the results of the work, not repeat them. A combined Results and Discussion section is often appropriate. Avoid extensive citations and discussion of published literature.

Conclusions
The main conclusions of the study may be presented in a short Conclusions section, which may stand alone or form a subsection of a Discussion or Results and Discussion section.

Appendices
If there is more than one appendix, they should be identified as A, B, etc. Formulae and equations in appendices should be given separate numbering: Eq. (A.1), Eq. (A.2), etc.; in a subsequent appendix, Eq. (B.1) and so on. This also applies to tables and figures: Table A.1; Fig. A.1, etc.

Essential title page information

Title. Concise, informative, and interesting. Titles are often used in information-retrieval systems. Avoid abbreviations and formulae where possible.

Author names and affiliations. Please clearly indicate the given name(s) and family name(s) of each author and check that all names are accurately spelled. Present the authors' affiliation addresses (where the actual work was done) below the names. Indicate all affiliations with a lower-case superscript number immediately after the author's name and in front of the appropriate address. Provide the full postal address of each affiliation, including the country name and, if available, the e-mail address of each author.

Corresponding author. Clearly indicate who will handle correspondence at all stages of refereeing, publication, and post-publication. Ensure that the e-mail address is given and that contact details are kept up to date by the corresponding author.

Present/permanent address. If an author has moved since the work described in the article was done, or was visiting at the time, a 'Present address' (or 'Permanent address') may be indicated as a footnote to that author's name. The address at which the author actually did the work must be retained as the main, affiliation address. Superscript Arabic numerals are used for such footnotes.

Abstract
A concise and factual abstract is required. The abstract should state briefly the purpose of the research, the principal

results and major conclusions. An abstract is often presented separately from the article, so it must be able to stand alone. For this reason, References should be avoided, but if essential, then cite the author(s) and year(s). Also, non-standard or uncommon abbreviations should be avoided, but if essential they must be defined at their first mention in the abstract itself.

Keywords

Immediately after the abstract, provide a maximum of 6 keywords, using American spelling and avoiding general and plural terms and multiple concepts (avoid, for example, 'and', 'of '). Be sparing with abbreviations: only abbreviations firmly established in the field may be eligible. These keywords will be used for indexing purposes.

Abbreviations

Define abbreviations that are not standard in this field in a footnote to be placed on the first page of the article. Such abbreviations that are unavoidable in the abstract must be de- fined at their first mention there, as well as in the footnote. Ensure consistency of abbreviations throughout the article.

Acknowledgements

Collate acknowledgements in a separate section at the end of the article before the references and do not, there- fore, include them on the title page, as a footnote to the title or otherwise. List here those individuals who provided help during the research (e.g., providing language help, writing assistance or proof reading the article, etc.), as well as institutions and funding agencies.

Units

Follow internationally accepted rules and conventions: use the international system of units (SI). If other units are mentioned, please give their equivalent in SI.

Math formulae

Please submit math equations as editable text and not as images. Present simple formulae in line with normal text where possible and use the solidus (/) instead of a horizontal line for small fractional terms, e.g., X/Y. In principle, variables are to be presented in italics. Powers of e are often more conveniently denoted by exp. Number consecutively any equations that have to be displayed separately from the text (if referred to explicitly in the text).

Electronic artwork
General points

Make sure you use uniform lettering and sizing of your original artwork.

Preferred fonts: Arial (or Helvetica), Times New Roman (or Times), Symbol, Courier.

Number the illustrations according to their sequence in the text.

Use a logical naming convention for your artwork files.

For Word submissions only, you may provide figures, their captions, and tables within a single file at the revision stage.

Formats
Regardless of the application used, when your electronic artwork is finalized, please 'save as' or convert the images to one of the following formats (note the resolution requirements for line drawings, halftones, and line/halftone combinations given below):

EPS (or PDF): Vector drawings. Embed the font or save the text as 'graphics'.

TIFF (or JPG): Color or grayscale photographs (half- tones): always use a minimum of 300 dpi.

TIFF (or JPG): Bitmapped line drawings: use a mini- mum of 1000 dpi.

TIFF (or JPG): Combined bitmapped line/half-tone (color or grayscale) images: a minimum of 500 dpi is required. **Please do not:**

Supply files that are optimized for screen use (e.g., GIF, BMP, PICT, WPG); the resolution is too low.

Supply files that are too low in resolution.

Submit graphics that are disproportionately large for the content.

Color artwork
Please make sure that artwork files are in an acceptable format — TIFF (or JPEG), EPS (or PDF), or MS Office files — and with the correct resolution. If, together with your accepted article, you submit usable color figures, the- se will appear in color online.

Figure captions
Ensure that each illustration has a caption. A caption should comprise a brief title (not on the figure itself) and a description of the illustration. Keep text in the illustrations to a minimum, but be sure to explain all symbols and abbreviations used.

Tables
Please submit tables as editable text and not as images. Tables can be placed either next to the relevant text in the article, or on separate page(s) at the end. Number tables consecutively in accordance with their appearance in the text and place any table notes below the table body. Be spa- ring in the use of tables and ensure that the data presented in them do not duplicate results described elsewhere in the article. Please avoid using vertical rules.

Citation in text
Please ensure that every reference cited in the text is also present in the reference list (and vice versa). Any references cited in the abstract must be given in full. Unpublished results and personal communications are not recommended in the reference list, but may be mentioned in the text. If

these references are included in the reference list they should follow the standard reference style of the journal and should include a substitution of the publication date with either 'Unpublished results' or 'Personal communication'. Citation of a reference as 'in press' implies that the item has been accepted for publication.

Web references
As a minimum, the full URL should be given and the date when the reference was last accessed. Any further information, if known (DOI, author names, dates, reference to a source publication, etc.), should also be given. Web references can be listed separately (e.g., after the reference list) under a different heading if desired, or can be included in the reference list.

Reference formatting
There are no strict requirements on reference format- ting at submission. References can be in any style or format as long as the style is consistent. Where applicable, name(s) of author(s), journal title/book title, chapter title/article title, year of publication, volume number/book chapter and the pagination must be present. Use of DOI is highly encouraged. The reference style used by the journal will be applied to the accepted article by SCIELO at the proof stage. Note that missing data will be highlighted at proof stage for the author to correct.

Reference style
All publications cited in the text should be presented in a list of references following the text of the manuscript. In the text refer to the author's name (without initials) and year of publication (e.g. "Since Almeida (1986) has shown that..." or "This is in agreement with results obtained later (Trompette 1994; Heilbron and Machado 2003)."
For three or more authors use the first author followed by "et al.", in the text. The list of references should be arranged alphabetically by authors' names. The manuscript should be carefully checked to ensure that the spelling of authors' names and dates are exactly the same in the text as in the reference list.
References should be given in the following form:

Papers in scientific journals

Almeida F.F.M. 1986. Distribuição regional e relações tectônicas do magmatismo pós-paleozóico no Brasil. *Revista Brasileira de Geociências*, **16:**325-349.

Costa I.P., Bueno G.V., Milhomem P.S., Silva H.S.R.L., Kosin M.D. 2007. Sub-bacia de Tucano Norte e Bacia de Jatobá. *Boletim de Geociências da Petrobras*, **15:**445-453.

Escayola M.P., Pimentel M.M., Armstrong R. 2007. Neoproterozoic backarc basin: sensitive high-resolution ion microprobe U-Pb and Sm-Nd isotopic evidence from the eastern Pampean Ranges, Argentina. *Geology*, **35:**495-498.

Heilbron, M. and Machado, N. 2003, Timing of terrane accretion in the Neoproterozoic-Eopaleozoic Ribeira orogen (SE Brazil). *Precambrian Research*, **125:**87-112.

Books and book chapters

Bedell R., Crósta A.P., Grunsky E. (eds.). 2009. *Remote Sensing and Spectral Geology*. Littleton, Society of Economic Geologists, 270 p.

Kaufman A.J., Sial A.N., Frimmel H.E., Misi A. 2009. Neoproterozoic to Cambrian palaeoclimatic events in southwestern Gondwana In: Gaucher C., Sial A.N., Frimmel H.E., Helverson G.P. (eds.). Neoproterozoic- Cambrian tectonics, global change and evolution: a focus on southwestern Gondwana. *Developments in Precambrian Geology*, 16, Amsterdam, Elsevier, p. 369-388.

Pankhurst R.J. & Rapela C.W. (eds.). 1998. The P*roto-Andean margin of Gondwana*. London, Geological Society of London Special Publication, **142**, 382 p.

Trompette R. 1994. *Geology of western Gondwana (2000–500 Ma)*. Rotterdam, Balkema, 350 p.

Papers in scientific meetings

Astini R., Ramos V.A., Benedetto J.L., Vaccari N.E., Cañas F.L. 1996. La Precordillera: un terreno exótico a Gondwana. In: 13°Congreso Geológico Argentino y 3° Congreso Exploración de Hidrocarburos. Buenos Aires, *Actas*, v. 5, p. 293-324.

Leite-Junior W.B, Bettencourt J.S., Payolla B.L. 2003. Evidence for multiple sources inferred from Sr and Nd isotopic data from felsic rocks in the Santa Clara Intrusive Suite, Rondonia, Brazil. In: SSAGI, South American Symposium on Isotope Geology. Salvador, *Short Papers*, p. 583-585.

Milani E.J. & Thomaz-Filho A. 2000. Sedimentary basins of South América. In: Cordani U.G., Milani E.J., Thomaz- Filho A., Campos D.A. (eds.). Tectonic evolution of South America. *31st International Geological Congress*. Rio de Janeiro, p. 389-452.

Thesis and dissertations

Paes V.J.C. 1999. *Geologia da quadrícula Alvarenga, MG, e a geoquímica:* implicações geotectônicas e metalogenéticas. MS Dissertation, Instituto de Geociências, Universidade Federal de Minas Gerais, Belo Horizonte, 144 p.

Ávila C.A. 2000. *Geologia, petrografia e geocronologia de corpos plutônicos paleoproterozóicos da borda meridional do Cráton São Francisco, região de São João Del Rei,*

Minas Gerais. PhD Thesis, Universidade Federal do Rio de Janeiro, Rio de Janeiro, 401 p.

Printed maps

Inda H.A.V. & Barbosa J.F. 1978. *Mapa geológico do Estado da Bahia, escala 1:1.000.000.* Salvador, Secretaria das Minas e Energia, Coordenação da Produção Mineral. Mascarenhas J.F. & Garcia T.M. 1989. *Mapa geocronológico do Estado da Bahia, escala 1:1.000.000.* Texto explicativo. Salvador, Secretaria das Minas e Energia, Coordenação da Produção Mineral, 186 p. Schobbenhaus C. (coord.). 1975. *Carta Geológica do Brasil ao Milionésimo – Folha Goiás (SD 22).* Texto explicativo. Brasília, Departamento Nacional da Produção Mineral, 114 p.

Internal reports
Internal reports will not be accepted, unless of open access for the scientific community and authorized by ad hoc consultants.

Submission checklist

The following list will be useful during the final checking of an article prior to sending it to the journal for review. Please consult this Guide for Authors for further details of any item. Ensure that the following items are present:
One author has been designated as the corresponding author with contact details:

E-mail address

Full postal address

All necessary files have been uploaded, and contain:

Keywords

All figure captions

All tables (including title, description, footnotes)

Further considerations:

Manuscript has been 'spell-checked' and 'grammar-checked'.

All references mentioned in the Reference list are cited in the text, and vice versa.

Permission has been obtained for use of copyrighted material from other sources (including the Internet).

Rapid communications
Rapid communications are limited to 2000 words, including references. Summary and abstract are limited to 100 words. At the discretion of the editors, these communications may be scheduled for the first available edition.

Articles with accelerated review process
An accelerated review process may be requested for complete original studies, for which urgency of publication is

adequately justified. At the discretion of the editors, these can be programmed for the first available edition. They must follow the same format described for original articles.

Editorials
Editorials should cover some aspect of the broad spectrum of the Geological Sciences. They will be authored by the editors of BJG, by people linked to the Brazilian Geological Society or by industry personalities. These documents will not be submitted to peer review and will be published at the discretion of the editors.

Review articles
Review articles should cover relevant topics of Geology. These articles may be requested by the editors, but recognized experts may spontaneously submit review articles in their field of expertise. In this case, potential authors should contact the editors to ascertain their interest prior to submitting the article

Manuscript submission

The submission of manuscripts must only be performed online at http://mc04.manuscriptcentral.com/bjgeo-scielo

There are no fees for submission and evaluation of articles.

ANEXO B – COMPROVANTE DE SUBMISSÃO DO ARTIGO

Brazilian Journal of Geology

BRAZILIAN JOURNAL OF GEOLOGY

GRAPHITE OCCURRENCES IN THE TANQUE NOVO - IPIRÁ COMPLEX, NORTHEAST OF THE SÃO FRANCISCO CRATON, BAHIA, BRAZIL: CHARACTERIZATION AND METALLOGENIC POTENTIAL